Application and Mechanism Characterization of Nanofibers for Interlaminar Toughening of Composite Materials

（層間強化におけるナノファイバーの応用とメカニズム解明）

By

Mingjun Shi

Gifu university

Graduate school of engineering

Mechanical and Civil engineering division

A thesis submitted for the degree of Doctor of Philosophy

Contents

Abstract

Composite materials, especially carbon fiber reinforced polymers, are becoming the materials of choice in weight-critical structural components due to their high specific strength and stiffness. Despite these attributes, the interlaminar regions between the individual plies are matrix-rich region, making them points of weakness. This results in interlaminar failure or delamination being a major disadvantage of composite laminates. These problems can be solved by adding particles to bulk resin or inserting films. However, these toughing methods have their drawbacks, like heterogeneous dispersion of particles in interlayer, and poor adhesion at resin/film interface. Recently, the method of improving delamination resistant by use of electrospun nanofiber veils as interleaves provide alternative options to remedy some defects of interlayer toughing method mentioned above due to the following advantages: porosity which makes resin flow easily through them without causing non-uniform dispersion of nanofiller, thinness and light which make their impact on weight and thickness of the final manufactured negligible. Many papers have been published regarding the nanofiber veils have an impressive effect on fracture and impact behavior of nano-modified laminate. However, for automobile and aerospace users, the fatigue performance of composites is of primary importance. Up to now, research on fatigue response of nano-modified laminates is still poor. In addition, the existing studies paid more attention to the application of electrospun nanofiber in strengthening the interlaminar of thermosetting resin-based composite laminate, whereas the thermoplastic resin-based composites laminate are more and more widely used since they possess characteristics of high-production efficiency and recyclability. Therefore, this study focuses on the following two aspects.

In the first aspect, the cross-ply laminate fabricated by vacuum-assisted resin transfer molding (VaRTM) was engaged in performing static and dynamic tests to reveal static and fatigue response of non-crimp fabric laminates modified with electrospun nanofiber veils. First, the ILSS tests and flexural tests were employed to investigate the static behavior of nano-modified laminates combined with optical micrographs of the fracture surface. The results of tests indicated the nanofiber toughing interlayer had a significant effect on improving the critical ILSS stress and flexural strength, attributed to the improved shear properties of the matrix-rich region and high-strain plastic deformation within nanofiber interlayer due to the reinforcement of the interlayer with the nanofiber veil. Notably, the nano-modified configurations showed almost the same flexural modulus as virgin configuration, and the ultimate flexural stress improved about 25.5%. Afterward, the fatigue tests were conducted under the load-control fatigue condition with R=0.25 and f=5HZ, the applied fatigue load was about 40%~90% of ultimate flexural stress The fatigue results showed that the nano-modified configurations had been in a mechanical state of high load and high deflection under the same percentage levels with virgin due to its high maximum critical load and same elastic modulus as the virgin configuration. The maximum stiffness reduction was only 10% compared with virgin stiffness reduction of 20% for the whole fatigue life based on the relative flexural stiffness (RFS) analysis. And through analysis of stiffness decrease rate obtained by linear regression of RFS-number of cycles curves, the stiffness of the nano-modified samples decreased significantly slower than that of the virgin samples at high-stress level, which enhanced the attractive effect of nanofiber interleaves on maintaining stiffness. Consequently, the fatigue strength of nano-modified configuration was 1.7

times higher than virgin configuration, and the run-out points analysis revealed that the nanofiber veil had great potential to extend the material fatigue stress range and optimize the capability of fatigue energy absorption for the composite material. Alternatively, the residual strength investigation clarified that higher fatigue loading caused more damage in material resulting in lower residual strength. However, the reduction of residual strength was independent with stiffness reduction.

In the second aspect, for the purpose of the nanofiber veil applied in the toughness enhancement of CFRTP, the sheets of PA polymeric nanofibers that were interleaved between consecutive layers of a PMMA-based laminate under appropriate hot-pressing conditions to improve the interlayer toughness of laminate. The Mode-I and Mode-II experiments verified that the inter-leaved PA veils had a considerable improvement in interlaminar fracture toughness of the CFRTPs laminate system as a consequence of the nanofiber bridge effect. Besides, the compatibility of PMMA resin is typically poor with PA nanofibers and CF fiber. While interfacial adhesion of polymer to CF and nanofiber is the key to realize the potential of interlayer toughing effect of PA nanofiber. This work was extended the experimental study for analysis of the effect of interfacial adhesion improvement on fracture toughness behavior of CFRTP laminate and mechanism by using functional monomer hydroxyethyl acrylamide (HEAA) with different molar concentration for copolymerization with methyl methacrylate (MMA). With the increase in HEAA polymerization from 0mol% to 5mol%, the interlayer toughing effect of PA veils exhibited a characteristic of decreasing first and then increasing under the Mode-I loading, which was related to the change of delamination path accompanied by the shifting of bridging mechanism; whereas for Mode-II loading

exhibited a characteristic of increasing first and then decreasing, which was related to the formation of multilayer microcrack in nano-toughing matrix layer. Moreover, to further understand the effect of interfacial adhesion on fracture mechanism, the fracture surfaces of fiber layer and nano-toughing matrix layer were examined in detail. The result showed the improvement of resin adhesion to carbon fiber and PA nanofiber, for the DCB samples, enhanced the interfacial strength between nano-toughing matrix layer and carbon fiber layer, and also greatly inhibited the CF and nanofiber pull out from matrix thereby reducing the bridging effect; for the ENF samples, it effectively enhanced shear stress transmission between nanofiber and matrix, coupled with the weakening of elastic modulus of resin made the fracture of nanofibers increased with the resin drawing deformation in the thickness direction, but it must be pointed out that excessive HEAA polymerization also made the resin too elastic, resulting in insufficient deformation strength.

Finally, the conclusion of this thesis was summarized, it can be found that the nanofiber veils are effective toughening materials. In addition, the research outline of effect of cold plasma surface treatment on toughening mechanisms responsible for crack resistance in thermoplastic nanofiber reinforced epoxies was proposed in future work.

Chapter 1.
Introduction

1.1. Background

In facing the issue of increasingly serious climate change, governments around the world have also launched stricter carbon emission regulations. Existing data show that 100 kg weight saving in each automotive leads to a reduction in CO_2 emission of 20 g/m, using carbon fiber reinforced plastics to make automotive parts is the main method to achieve the car-light weighing for automotive manufacturers [1]. However, owning no reinforcement in thickness direction of the laminate, the characteristics of matrix determine mainly the out-plan behavior of laminate. Therefore, low damage resistance of composite laminate with thin resin-rich interfaces between adjacent layers is sensitive to failure that is likely to cause some of the primary damage forms of interlaminar delamination, transverse matrix crack, intralaminar delamination under the various loading. These possibly act as a trigger for a loss of load-carrying capacity between layers, which give rise to speed up the growth of damage and premature failure.

As such, a considerable number of researchers have devoted their attention to improving damage resistance by modifying construction and constituent materials used in the composite. Stitching is thinking about an effective way to join composite laminate piles through the use of various thread materials, experiment results proved obviously lifting of the tensile strength of stitched laminates compared to unstitched laminates, this was owing to energy absorption of stitch fibers in the process of fiber fracture and frictional pull-out; but having said that, due to stitching operation often incur in-plane fiber misalignment, fiber breakage and resin pockets, the in-plane modulus of stitched laminates is often lower than unstitched [2–4].

An alternative approach to enhance fracture toughness is interlaminar modifications. On the one hand, using the thermoplastic film interleaving is vailed an effective way to increase the delamination cracking resistance in laminates, owning to the effect of film plastic deformation and film bridging [5], yet an adverse effect on some mechanical properties of the laminate should be pointed out such as low tensile strength and low bending stiffness [6], and the interleaving films also can result in poor resin flow and poor adhesion at resin/film interface [7][8]. On the other hand, some researchers paid attention to stiff particles added to the resin to toughen the interlayer of laminate, it is proofed interlayer zones formed by particles modified matrix could significantly suppress delamination through crack path defection and crack-tip shielding mechanisms [9], but some disadvantage aspects, such as increasing resin viscosity, heterogeneous dispersion of particles due to filtering effects by fibers during the infusion process, cannot be neglected [10–13].

Compared with the methods of delamination resistant improving mentioned above, recently an interesting approach in the use of electrospun nanofiber veils as interleaves have attracted much attention, because nanofiber veils show super well mechanical properties of nanofibers including high modulus, high tensile strength, and toughness [14] and a nice infusion process by the porous feature and homogeneous distribution of veils in interlayers, that ensures the overall mechanical properties of composites [7,15–17]. Moreover, from compress test show that the nanofiber veil as interleaves inside a fabric laminate was more compressible than a plain electrospun veil, which can be explained as the nanofibers penetrating between carbon fibers during compression

process in composite manufacturing; thus, it is possible to improve the toughness of laminate toughness effectively [18].

Several excellent reviews describing the nanofiber veil exhibit good performance on improving Mode-I and Mode-II interlaminar fracture toughness of composites [7,17–22], Beckermann GW and Pickering KL found that the polymer type and areal weight of nanofiber veil were the most important factors affecting the properties of interleaved laminate [20]. Brugo T and Palazzetti R focus on the effect of the thickness of the nanotoughed layer on two types of laminae: unidirectional and plain wave; the general better results have been found for plain wave samples with thicker nanotoughed layer under the Mode-I load [21]. The material selection of reinforcement and the number of lay-up also affect the effectiveness of the interlayer toughness enhancement; results showed the nanofiber interleaves were less prominent for toughness enhancement for thicker glass fiber laminate [22]. Moreover, it is well known that the laminate composite exhibits poor impact tolerance, and some authors clarify that reason for the development of nanofiber bridging zones, more energy was absorbed by the nanofibers in the interleaved laminates [23,24].

As mentioned before, Mode-I, Mode-II, and impact testing have covered almost all the main aspects and provided a solid knowledge to understanding how the reinforcement mechanism of nanofiber interleaves act on the interlaminar fracture toughness of laminate. However, the fatigue performance of composites is critical for the automobile and aerospace industries. There is a knowledge gap regarding the flexural fatigue behavior of the nanofiber veil toughed composite [25,26]. In addition, the stiffness reduction caused by matrix crack is higher than that caused by other failure

mechanisms, such as fiber breakage and splitting of the 0° plies, in cross-ply laminates [27]. Therefore, the fatigue life of carbon fiber reinforced plastics is mainly determined by the crack resistance of the polymer matrix [28]. Several reported strategies to enhance the fatigue resistance of resin are focused on the modification of the polymer matrix, including adding carbon nanotubes [29], rubber [30], etc. Another reinforcement method is to introduce nanofibers into the rich resin region between the layers to form a new fiber-reinforced resin structure. Compared with the polymer matrix modification, this method does not change the viscosity of the resin and also provides excellent production convenience and operability.

Although thermosetting carbon fiber composites (CFRPs) based on HP-RTM molding technology have been widely used in some luxury cars, the technical defects of low-production efficiency and low-material recyclability limit the application of CFRPs in medium-end and low-end models. Thus, thermoplastic carbon fiber composites (CFRTPs) provide alternative options to remedy some defects of CFRPs [31,32]. As we all know, laminate composite materials are much liable to interply delamination due to their layup structure [33,34]. In the last 20 years, the electrospun nanofiber veils had been proven the ideal reinforcement to be interleaved between two piles of CFRPs because of the following main aspects: thinness and light which make their impact on weight and thickness of the final manufactured negligible; porosity which makes resin flow easily through them without causing nonuniform dispersion of nanofiller; tiny volume which means the actual volume of the nanofiber interleaves shrinks when pressure applied during the curing process; super well mechanical property due to nanofibers' mechanical properties is significantly higher than those of

the same material in bulk state[14]. From the research of various aspects of electrospun nanofiber reinforced thermoplastic resin [35–38], electrospun nanofiber can enhance the damage resistant of CFRTPs laminate system potentially. To the best knowledge of the authors. These possibilities remain to be explored.

Furthermore, it is also noted that from most observations of the fracture surface, the nanofiber fracture mechanism consistently exhibits pull-out mode without causing apparent damage to the nanofibers and the obvious interface separation between nanofiber and resin [39–43]. These observations suffice to illustrate that the compatibility between the majority of the thermoplastic veils and resin is typically poor. Moreover, the traditional active methods such as corona discharge, plasma treatment, acid etches, and oxidizing flame treatment could create severe damage to the nanofiber. There is no denying that one of the significant challenges for adhesion improvement is surface treatment methods for thermoplastic nanofiber veils. Recently, Dong et al. [44] proposed to employ a UV-irradiation technique to activate the surface of the nanofiber veils to improve their adhesion with epoxies. It was found that the application of the UV-irradiation to PPS veils significantly improved the toughness performance of the laminate manufactured by resin transfer molding of non-crimp fabrics by introducing significant carbon delamination and PPS fiber damage during the fracture process. On the other hand, the semi-cured epoxy resin in the UD prepreg has a small number of reactive groups to covalently bond to the functional groups of UV-treated PPS surface, which could negatively affect the compatibility between the nanofibers and epoxy, leading to the deterioration of the fracture behavior of UD prepregs laminates. This

suggests that the thermoplastic nanofiber surface treatment has a significant effect on the interlayer toughing of laminates with different resin systems.

1.2. Main objectives of research

In order to remedy the research gap of fatigue behavior of nanofiber veil toughened composites and expending the application of nanofiber in interlaminar toughing of the CFRTP laminates system.

Some specific objectives of this research are:

- To examine static flexural behavior of nanofiber veils interleaved cross-ply CRTP laminates by interlaminar shear stress test (ILSS) and 3-points flexural tests, base materials were selected non-crimped carbon fibers. The interleaf veils were used polyamide (PA), at the meantime, in order to clarify the changes in failure mechanisms of cross-ply CRTP laminates bring about by nanointerleaves, the optical micrographs of fracture surfaces and cross-sections of damaged laminates were engaged to investigate..
- To clarify the static flexural progressive damage behavior of nanofiber interlayed cross-ply CRTP laminates, the interrupt 3point bending tests were conducted, and the fracture surface take from microscopy was used to monitor the crack progression.
- To perform fatigue tests on the virgin and interleaved specimens, the fatigue tests were conducted under the load-control fatigue condition and progressive damage in the material, which was continuously monitored by an increment of deflection.

- To analyze damage accumulation in different laminates, the fatigue behavior with interleaf veils is evaluated and discussed using the results of tests based on the viewpoint of fatigue modulus reduction.
- To examine the effectiveness of interlaminar toughening of PA nanofiber on the static flexural behavior of the CFRTP laminate system, the 3 points flexural bending tests were conducted on specimen with/without nanofiber. base materials were selected non-crimped carbon fibers. The interleaf veils were used polyamide.
- To examine the effectiveness of interlaminar toughening of PA nanofiber on the interlaminar fracture behavior of the CFRTP laminate system, the Mode-I and Mode-II tests were conductied,
- To improve the interfacial adhesion of resin to nanofiber and carbon fiber (CF) to further improve the toughing effect of PA nanofiber, the different molar concentrations of the functional monomer hydroxyethyl acrylamide (HEAA) was copolymerized with methyl methacrylate (MMA).
- To analyze the fracture mechanisms of nanofiber toughed CFRTP under Mode-I and Mode-II load conditions, the SEM photos were taken from the fracture surface were employed to investigate.
- To give suggestions for the future work based on existing work, and make a feasibility analysis for future work according to the literature review.

1.3. Outline of thesis

This thesis consists of eight chapters. Chapter 1 was an introduction to the background of the methods of improving delamination resistance and the previous work

about the application of nanofiber interleafing to highlight the importance of our works. Subsequently, this chapter briefly explained the objectives of this work and the construction of this thesis.

Chapter 2 reported on the static flexural tests. Two types of cross-ply laminates systems were fabricated as testing specimens: virgin configuration and NM configuration. The PA nanofiber veils as interleaf material were inserted in each interface between 0°- and 90°- oriented plies. The interlaminar shear stress and flexural stress were measured using the 3-points bending test. Firstly the ILSS behavior and flexural behavior were illustrated and summarized. Then the mechanisms of the nanofiber interlayer were evaluated and combined the micrographic photo of the edge fracture surface. Chapter 3 statically evaluated the static flexural progressive damage behavior of nanofiber interlayered laminate through the edge observations and discussed the mechanism change of cracking brought out by nanofiber toughed interlayer.

The fatigue behavior of interlaminar toughening by the PA nanofiber was discussed in chapter 4. The 3-point bending tests were carried out for fatigue tests, and the same materials as the static flexural tests were used. Fatigue behavior was illustrated firstly, then based on the viewpoint of fatigue modulus reduction, the stiffness degradation in different laminates was analyzed. Finally, the precycling specimens (run-out with 10^6) were tested again to clarify the residual stress.

Due to the less application of nanofiber interlayer toughing for CFRTP, Chapter 5 firstly discussed the effect of nanofiber interleaving on the static behavior of CFRTP composite through the static bending test. Then, in order to clarify the effect of

nanofiber interlaminar toughening on interlaminar fracture behavior of CFRTP laminate system. Chapter 6 presented the Mode-I interlaminar toughness tests. The unidirectional non-crimped carbon fibers and four types of resin were chosen as the base material. The test configurations consisted of five types, including virgin and nanomodification. Mode-I energy release rate G_I was measured using the DCB test. Firstly the G for all specimens was illustrated and summarized; in the discussion section, the effect of interfacial adhesion improvement of fiber/matrix on mechanisms of the Mode-I toughness by the interleaf veils was discussed.

Chapter 7 showed Mode-II interlaminar toughening by the PA nanofiber; for the Mode-II tests, the ENF test was implemented, and the same materials as the Mode-I were used. The construction of the chapter 7 is almost the same as chapter 6. Resistance curves and Mode-II energy release rate value G_{II} were illustrated and explained in the result section. The mechanisms of the Mode-II interlaminar toughness were discussed.

In chapter 8, the conclusion of the research was summarized. All specimen fabrication and test programs had been summarized. And the most important is the combination of this study systematically expounds on the critical role of nanofibers for interlayer toughening.

The toughness mechanisms of laminate systems have been investigated by many methods and aspects. Of course, improvement of toughening techniques for the composite materials is still developing. Chapter 8 also given out a suggestion for future work.

References

[1] Ishikawa T, Amaoka K, Masubuchi Y, et al. Overview of automotive structural composites technology developments in Japan. Compos Sci Technol [Internet]. 2018;155:221–246. Available from: https://doi.org/10.1016/j.compscitech.2017.09.015.

[2] Zheng Y, Cheng X, Yasir B. Effect of stitching on plain and open-hole strength of CFRP laminates. Chinese J Aeronaut [Internet]. 2012;25:473–484. Available from: http://dx.doi.org/10.1016/S1000-9361(11)60411-1.

[3] Tan KT, Watanabe N, Iwahori Y. Experimental investigation of bridging law for single stitch fibre using Interlaminar tension test. Compos Struct [Internet]. 2010;92:1399–1409. Available from: http://dx.doi.org/10.1016/j.compstruct.2009.11.018.

[4] Tan KT, Watanabe N, Iwahori Y, et al. Effect of stitch density and stitch thread thickness on compression after impact strength and response of stitched composites. Compos Sci Technol [Internet]. 2012;72:587–598. Available from: http://dx.doi.org/10.1016/j.compscitech.2012.01.003.

[5] Li L, Lee-Sullivan P, Liew KM. The influence of thermoplastic film interleaving on the interlaminar shear strength and mode i fracture of laminated composites. J Eng Mater Technol Trans ASME. 1996;118:302–309.

[6] Kim JW, Lee JS. Influence of interleaved films on the mechanical properties of carbon fiber fabric/polypropylene thermoplastic composites. Materials (Basel). 2016;9.

[7] van der Heijden S, Daelemans L, Meireman T, et al. Interlaminar toughening of resin transfer molded laminates by electrospun polycaprolactone structures:

Effect of the interleave morphology. Compos Sci Technol [Internet]. 2016;136:10–17. Available from: http://dx.doi.org/10.1016/j.compscitech.2016.09.024.

[8] Hojo M, Matsuda S, Tanaka M, et al. Mode I delamination fatigue properties of interlayer-toughened CF/epoxy laminates. Compos Sci Technol. 2006;66:665–675.

[9] Gao F, Jiao G, Lu Z, et al. Mode II delamination and damage resistance of carbon/epoxy composite laminates interleaved with thermoplastic particles. J Compos Mater. 2007;41:111–123.

[10] Liu L, Huang ZM, He CL, et al. Mechanical performance of laminated composites incorporated with nanofibrous membranes. Mater Sci Eng A. 2006;435–436:309–317.

[11] Wong DWY, Lin L, McGrail PT, et al. Improved fracture toughness of carbon fibre/epoxy composite laminates using dissolvable thermoplastic fibres. Compos Part A Appl Sci Manuf [Internet]. 2010;41:759–767. Available from: http://dx.doi.org/10.1016/j.compositesa.2010.02.008.

[12] Kamaraj M, Dodson EA, Datta S. Effect of graphene on the properties of flax fabric reinforced epoxy composites. Adv Compos Mater [Internet]. 2020;29:443–458. Available from: https://doi.org/10.1080/09243046.2019.1709679.

[13] Ahmad W, Dey B, Sammar AA, et al. In situ synthesis of graphene oxide in multi-walled carbon nanotube hybrid-reinforced polyetherimide nanocomposites with improved electrical, mechanical and thermal properties. Adv Compos Mater [Internet]. 2020;29:529–546. Available from:

https://doi.org/10.1080/09243046.2019.1710680.

[14] Jiang S, Chen Y, Duan G, et al. Electrospun nanofiber reinforced composites: A review. Polym Chem. 2018;9:2685–2720.

[15] Zucchelli A, Focarete ML, Gualandi C, et al. Electrospun nanofibers for enhancing structural performance of composite materials. Polym Adv Technol. 2011;22:339–349.

[16] Boon Y Di, Joshi SC. A review of methods for improving interlaminar interfaces and fracture toughness of laminated composites. Mater Today Commun [Internet]. 2020;22:100830. Available from: https://doi.org/10.1016/j.mtcomm.2019.100830.

[17] Barkoula NM, Alcock B, Cabrera NO, et al. Influence of Geometrical Features of Electrospun Nylon 6,6 Interleave on the CFRP Laminates Mechanical Properties with Graphene. Polym Polym Compos. 2008;16:101–113.

[18] Daelemans L, Van Der Heijden S, De Baere I, et al. Damage-Resistant Composites Using Electrospun Nanofibers: A Multiscale Analysis of the Toughening Mechanisms. ACS Appl Mater Interfaces. 2016;8:11806–11818.

[19] Ramirez VA, Hogg PJ, Sampson WW. The influence of the nonwoven veil architectures on interlaminar fracture toughness of interleaved composites. Compos Sci Technol [Internet]. 2015;110:103–110. Available from: http://dx.doi.org/10.1016/j.compscitech.2015.01.016.

[20] Beckermann GW, Pickering KL. Mode i and Mode II interlaminar fracture toughness of composite laminates interleaved with electrospun nanofibre veils. Compos Part A Appl Sci Manuf. 2015;72:11–21.

[21] Brugo T, Palazzetti R. The effect of thickness of Nylon 6,6 nanofibrous mat on Modes I–II fracture mechanics of UD and woven composite laminates. Compos Struct. 2016;154:172–178.

[22] Palazzetti R. Flexural behavior of carbon and glass fiber composite laminates reinforced with Nylon 6,6 electrospun nanofibers. J Compos Mater. 2015;49:3407–3413.

[23] Daelemans L, Cohades A, Meireman T, et al. Electrospun nanofibrous interleaves for improved low velocity impact resistance of glass fibre reinforced composite laminates. Mater Des [Internet]. 2018;141:170–184. Available from: https://doi.org/10.1016/j.matdes.2017.12.045.

[24] Shivakumar K, Chen H, Akangah P, et al. Polymer nanofabric interleaved composite laminates. 24th Annu Tech Conf Am Soc Compos 2009 1st Jt Can Tech Conf Compos. 2009;3:1608–1621.

[25] Beckermann GW. Nanofiber interleaving veils for improving the performance of composite laminates. Reinf Plast [Internet]. 2017;61:289–293. Available from: http://dx.doi.org/10.1016/j.repl.2017.03.006.

[26] Palazzetti R, Zucchelli A. Electrospun nanofibers as reinforcement for composite laminates materials – A review. Compos Struct [Internet]. 2017;182:711–727. Available from: https://doi.org/10.1016/j.compstruct.2017.09.021.

[27] S. L. Ogin PAS and PWRB. Matrix Cracking and Stiffness Reduction during the Fatigue of a (0/90)s GFRP Laminate. Compos Sci Technol. 1985;22:23–31.

[28] Harris, Bryan. Fatigue in composites: science and technology of the fatigue response of fibre-reinforced plastics. Woodhead Publishing; 2003.

[29] Wang GT, Liu HY, Saintier N, et al. Cyclic fatigue of polymer nanocomposites. Eng Fail Anal [Internet]. 2009;16:2635–2645. Available from: http://dx.doi.org/10.1016/j.engfailanal.2009.04.022.

[30] Quan D, Ivankovic A. Effect of core-shell rubber (CSR) nano-particles on mechanical properties and fracture toughness of an epoxy polymer. Polymer (Guildf) [Internet]. 2015;66:16–28. Available from: http://dx.doi.org/10.1016/j.polymer.2015.04.002.

[31] Wan Y, Takahashi J. Deconsolidation behavior of carbon fiber reinforced thermoplastics. J Reinf Plast Compos. 2014;33:1613–1624.

[32] Yanagimoto J, Ikeuchi K. Sheet forming process of carbon fiber reinforced plastics for lightweight parts. CIRP Ann - Manuf Technol [Internet]. 2012;61:247–250. Available from: http://dx.doi.org/10.1016/j.cirp.2012.03.129.

[33] Dikshit V, Bhudolia SK, Joshi SC. Multiscale polymer composites: A review of the interlaminar fracture toughness improvement. Fibers. 2017;5.

[34] Sato N, Hojo M, Nishikawa M. Intralaminar fatigue crack growth properties of conventional and interlayer toughened CFRP laminate under mode i loading. Compos Part A Appl Sci Manuf [Internet]. 2015;68:202–211. Available from: http://dx.doi.org/10.1016/j.compositesa.2014.09.031.

[35] Gonçalves NI, Münchow EA, Santos JD, et al. The role of polymeric nanofibers on the mechanical behavior of polymethyl methacrylate resin. J Mech Behav Biomed Mater. 2020;112.

[36] Li B, Yuan H, Zhang Y. Transparent PMMA-based nanocomposite using electrospun graphene-incorporated PA-6 nanofibers as the reinforcement.

Compos Sci Technol. 2013;89:134–141.

[37] Jiang S, Duan G, Hou H, et al. Novel layer-by-layer procedure for making nylon-6 nanofiber reinforced high strength, tough, and transparent thermoplastic polyurethane composites. ACS Appl Mater Interfaces. 2012;4:4366–4372.

[38] Li B, Pan S, Yuan H, et al. Optical and mechanical anisotropies of aligned electrospun nanofibers reinforced transparent PMMA nanocomposites. Compos Part A Appl Sci Manuf [Internet]. 2016;90:380–389. Available from: http://dx.doi.org/10.1016/j.compositesa.2016.07.024.

[39] Beylergil B, Tanoğlu M, Aktaş E. Enhancement of interlaminar fracture toughness of carbon fiber–epoxy composites using polyamide-6,6 electrospun nanofibers. J Appl Polym Sci. 2017;134:1–12.

[40] Del Saz-Orozco B, Ray D, Stanley WF. Effect of thermoplastic veils on interlaminar fracture toughness of a glass fiber/vinyl ester composite. Polym Compos. 2017;38:2501–2508.

[41] O'Donovan K, Ray D, McCarthy MA. Toughening effects of interleaved nylon veils on glass fabric/low-styrene-emission unsaturated polyester resin composites. J Appl Polym Sci. 2015;132:1–9.

[42] Kuwata M, Hogg PJ. Interlaminar toughness of interleaved CFRP using non-woven veils: Part 1. Mode-I testing. Compos Part A Appl Sci Manuf [Internet]. 2011;42:1551–1559. Available from: http://dx.doi.org/10.1016/j.compositesa.2011.07.016.

[43] Nash NH, Ray D, Young TM, et al. The influence of hydrothermal conditioning on the Mode-I, thermal and flexural properties of Carbon/Benzoxazine

composites with a thermoplastic toughening interlayer. Compos Part A Appl Sci Manuf [Internet]. 2015;76:135–144. Available from: http://dx.doi.org/10.1016/j.compositesa.2015.04.023.

[44] Quan D, Deegan B, Alderliesten R, et al. The influence of interlayer/epoxy adhesion on the mode-I and mode-II fracture response of carbon fibre/epoxy composites interleaved with thermoplastic veils. Mater Des. 2020;192:1–10.

Chapter 2.

Experimental study on static flexural behavior of nanofiber interlayered cross-ply non-crimp fabric composites.

2.1. Introduction

In this chapter, the main objective was to investigate the influence of the nanofiber interleaf on the static mechanical properties of non-crimp fabric lay-up laminate by interlaminar shear tests (ILSS) and static flexural tests. The laminate systems, including virgin configuration and nanomodified configuration, could be fabricated by the VaRTM technique. The photos of fracture surface in cross-section were observed by microscopy. The static results combined with optical micrographs of fracture surfaces were to clarify the changes in failure mechanism brought by nano-interleaves.

2.2. Experiments

2.2.1. Material information

The unidirectional non-crimp carbon fabrics with an areal weight of 793 g/m^2 supplied by Hokuriku Fiberglass Ltd (Ishikawa, Japan) were used, and the dry ply thickness was approximately 0.7 mm. The epomount epoxy resin with hardener produced by Refinetec Ltd (Yokohama, Japan) was used. Electrospun nanofiber veils, called Xantu.Layr XLB, with an areal density of 4 g/mm^2 were supplied by Revolution Fibres Ltd (Auckland, New Zealand). The composition of nanofibers was PA-XD10 produced by Mitsubishi Gas Chemical Inc (Tokyo, Japan), see in Fig. 1.

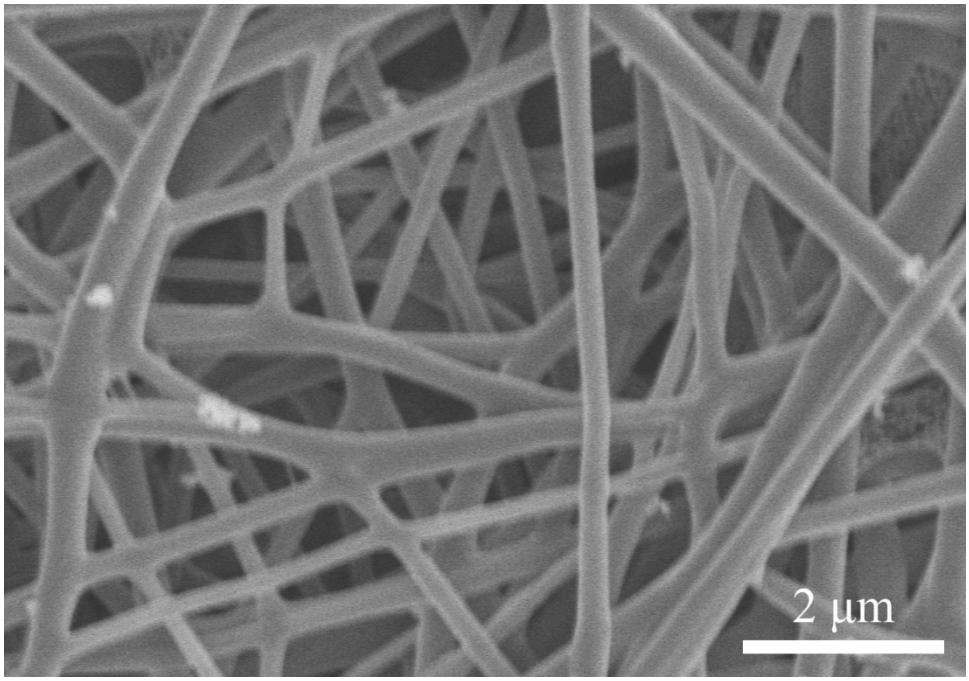

Fig. 1 Scanning electron micrographs of electrospun nanofiber veils

2.2.2. Composite preparation

Carbon fiber composite laminates were produced by VaRTM. A glass plate coated with a layer of mold release agent was used as a mold for flat laminates, the fabrics and interleaf veils were cut into 200 mm × 200 mm squares and laid up in two main configurations: virgin-$[0/90]_s$, nanomodified(NM)-$[0/90]_s$, in which the nanofiber veils were inserted in each interface between 0°- and 90°- oriented plies for nanofiber interleaved plates. Then the peel ply, the flow media, and the vacuum bag were set on the lay-up, epoxy resin was infused into the dry fabric and cured at room temperature, followed by a post-cure at room temperature for 24h. Specimens were cut from each laminate with a water-cooled diamond cutting machine. The edges of the specimens were polished to capture damage mechanisms by using optical microscopy.

The constructions of virgin and NM samples was shown in Fig. 2, the fiber-free zones (resin-rich zones), such as diamond-like shapes surrounding fiber yarns (called “opening”) in 90° ply or continuous “channel” in the interlayer of 0°/90°, can be

identified from the virgin laminate. These resin-rich zones were attributed to the deviation of the fibers from their uniform direction by stitching (warp knitted) loop. Moreover, the cross-ply laminate of the thick ply non-crimp carbon fabric is prone to crack formation in 90° ply under flexural loading [45]. The interleaved nanofiber layer was in the "channel" resin-rich zone of 0°/90° interlayer for the nanofiber laminate. This structural change in laminate affects their mechanical performance.

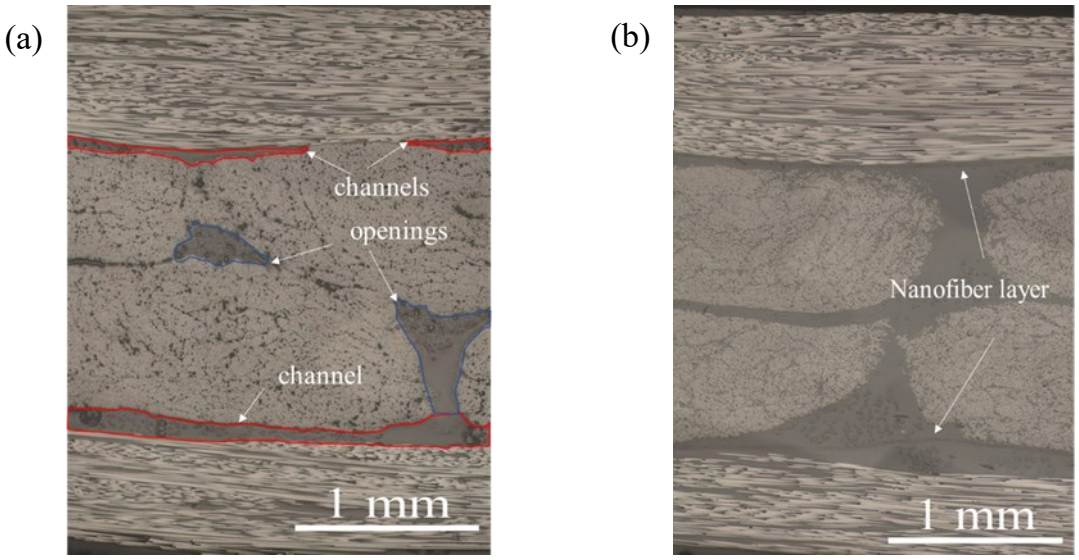

Fig. 2 Micrograph of non-crimp fabric cross-ply laminate structure in cross-section. (a) virgin composite (b) nanofiber modified composite.

2.2.3. Characterizations

Flexural test was conducted using the three-point bending apparatus (Fig. 3). Table 1 presents the specimen dimensions for different test types. Short-beam shear tests were applied to determine the interlaminar shear strength (ILSS). According to the simple beam theory for 3-point bending of rectangular geometry, the maximum interlaminar shear stress is gained at midplane thickness, the support span of the ILSS test is minimized to maximize the shear tensions. A span to medium thickness ratio was set at 5. The tests were conducted on a universal electromechanical testing machine at a fixed

loading rate of 1 mm/min based on the recommendation of the JIS7074 standard [46]. Meanwhile, the 3-point bending tests were performed in the same laboratory instrument as the ILSS test, with a 5 mm/min head displacement. Each type of experiment was tested with five samples.

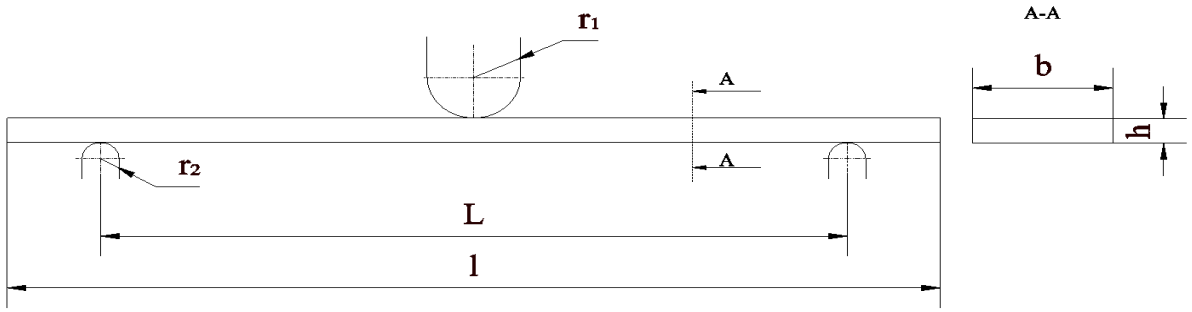

Fig. 3 Schematic view of the three-point bending apparatus.

Table 1. Specimen dimensions for different test types.

Test method	l[mm]	L[mm]	b[mm]	h[mm]	r_1[mm]	r_2[mm]	Test standard
Short-beam shear test	30	15	15	2.87	5	2	JIS K7057:2006
Flexural bending test	150	113	15	2.95	5	2	Lab condition

2.3. Results and discussions

2.3.1. ILSS

The interlaminar shear stress was determined by the following equation:

$$\tau_{ILSS} = \frac{3P}{4bh}$$

where P was the load value when the load first drops, b was the width of specimen measured, and h was the thickness of specimen measured.

The ILSS properties of the virgin and NM composites were obtained by short-beam tests. Typical interlaminar shear stress-displacement curves for both configurations

were plotted in Fig. 4. The primary nonlinear exterior of curves may be a spurious region, which can be caused by the seating of the specimen [47]. All specimens showed that the load increases linearly with the displacement over the rest of the curve until it reaches a maximum value.

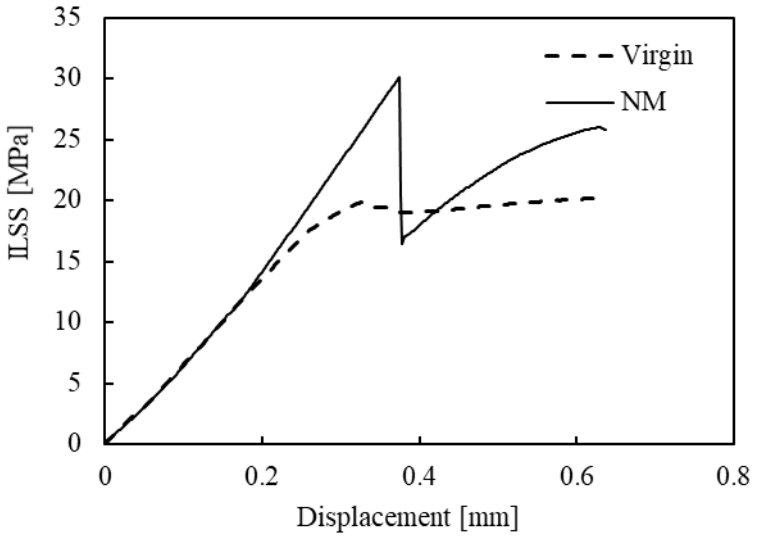

Fig. 4. Typical load-displacement curves during the ILSS test of $[0/90]_s$ cross-ply laminates.

The NM samples exhibited about 37% higher interlaminar shear strength than the virgin ones (Table 2). Fig. 4 shows that the NM samples exhibited brittle fracture behavior when the maximum critical stress was reached, whereas the load for the virgin samples almost kept a flat trend after attaining peak stress. The micrographs of the side fracture surfaces after the short-beam shear tests were observed to understand the mechanism responsible for the nanofiber veils enhancement of ILSS (Fig. 5). There were noticeable differences in fracture morphology between the composites with and without nanofiber veils. The matrix crack in the virgin ones typically expanded along the multi-direction in the inner core of the 90° layer, indicating cross-sectional shear mode and debonding being a primary mode of failure due to low-strain rigid

deformation of the matrix-rich region (Fig. 5 (b)). In contrast, a single directional crack that passed through the 90° ply thickness and run along the interlayer of 0°/90 in a long distance can be identified, indicating interlaminar shear mode and the interlaminar failure occurring mainly due to resin cracking and high-strain plastic deformation within the nanofiber interlayer (Fig. 5 (a)). The nanofiber veils present in the interleaf functioned as reinforcement for the matrix-rich interlayer and promoted matrix shear properties by offering resistance to matrix cracks, as evidenced by the high crack Mode I and Mode II initiation critical strain energy release rates for nanofiber interlayer reported in [20]. However, the lack of compatibility between nylon and epoxy [18,48] led to the propagation of cracks at the nanofiber-toughened layer interface (Fig. 5(a)); meanwhile, the Mode II and Mode I propagation strain energy release rates decreased rapidly as the crack moved into the less tough intralaminar zones [20][49], which explains the observation of the long distance crack can be observed in the interface between the nanofiber reinforced layer and matrix-rich layer (Fig. 5 (a)).

Table 2.Averaged ILSS and flexural properties of different laminates.

Lay-up		τ_{ILSS}[MPa]	σ_f[MPa]	E_f[GPa]
$[0/90]_s$	-virgin	20.47	664.1	80.4
	-NM	28.11	833.4	80.84

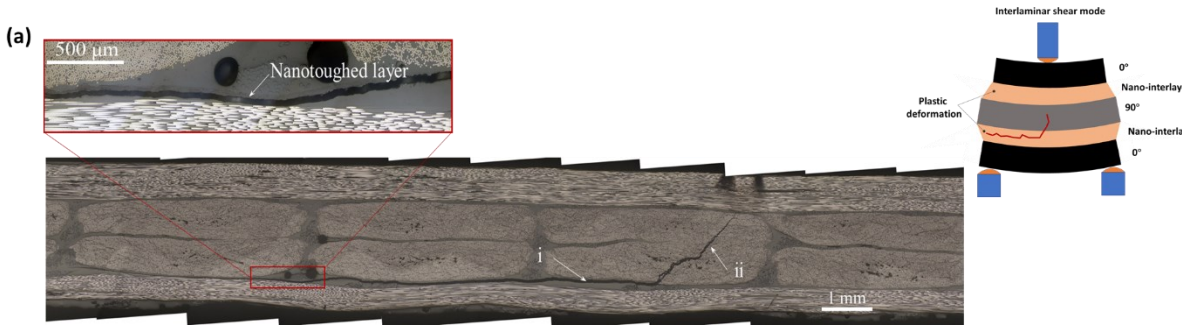

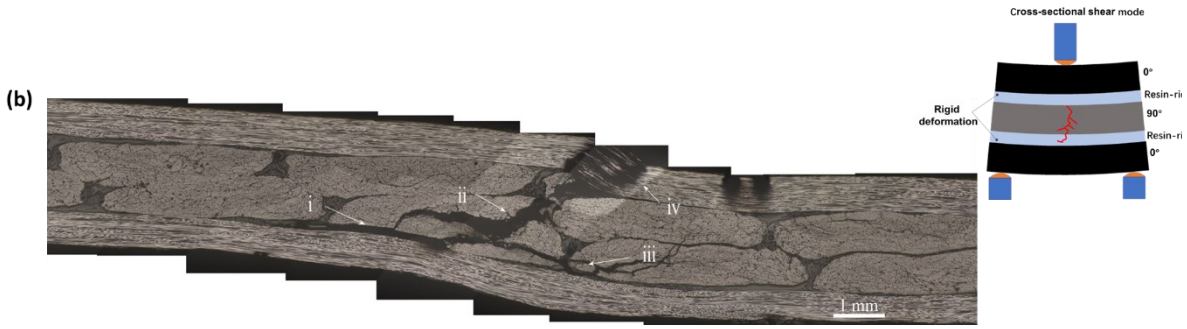

Fig. 5. Identification of failure modes for (a) $[0/90]_s$-nanomodified laminates and (b) $[0/90]_s$-virgin laminates in ILSS tests; (I) interlamination delamination, (II) transverse interlaminar matrix crack, (III) intralaminar delamination, (IV) fiber distortion associated with low shear stress.

2.3.2. Flexural test

A series of 3-point bending tests were conducted on the virgin and NM samples to investigate the interlaminar reinforcement effect of nanofiber veil on the flexural properties and their bulk failure mode. Fig. 6 presents the typical flexural stress-strain curve of cross-ply laminates. Although the flexural stress of the NM laminate increased at almost the same flexural modulus as the virgin ones, the UFS improvement was about 25.5% (Table 2). Fig. 7 shows the examined flexural failure surface. The damage initiation was observed to start in the upper 0° ply of the virgin sample under compressive loading. Several sites of intralaminar delamination occurred in the 0° ply due to local buckling in the fiber direction. Further, the typical shear failure mode with matrix cracking developed in the 90° ply (Fig. 7 (b)) with a rapid damage process (Fig. 6). These observations were in accordance with the trends observed in previous studies [50][51]. However, the failure of NM samples occurred in two stress leves (Fig. 6). For the first critical flexural stress level, the failure of fiber breakage occurred in 0° ply without the 0° intralaminar delamination, which could be explained by the fact that the beneficial effects of nanofibers were attributed to their energy-absorption behavior and

to the fact that they transfer the load toward the carbon fiber, thus reducing stress concentrations[26,52]. In addition, the crack reached the nanofiber-toughened layer; since the loads required to initiate crack propagation in the toughened interlayer regions with Mode II and Mode I failures were high [20], the critical flexural stress increased to a higher level. Finally, the crack rapidly propagated for a long distance at the interface of the nanofiber-toughened layer (Fig. 7(a)), which was attributed to the same reason as the ILSS failure. Further, the crack could not path through the nanofiber-toughened layer to form the matrix crack in 90° ply. This phenomenon was attributed to the significance of energy required to initiate cracks in the nanofiber-toughened epoxy, i.e., toughening mechanisms acting in the fracture processing zone in front of the crack tip, which was investigated in the single edge notched bending (SENB) test [18].

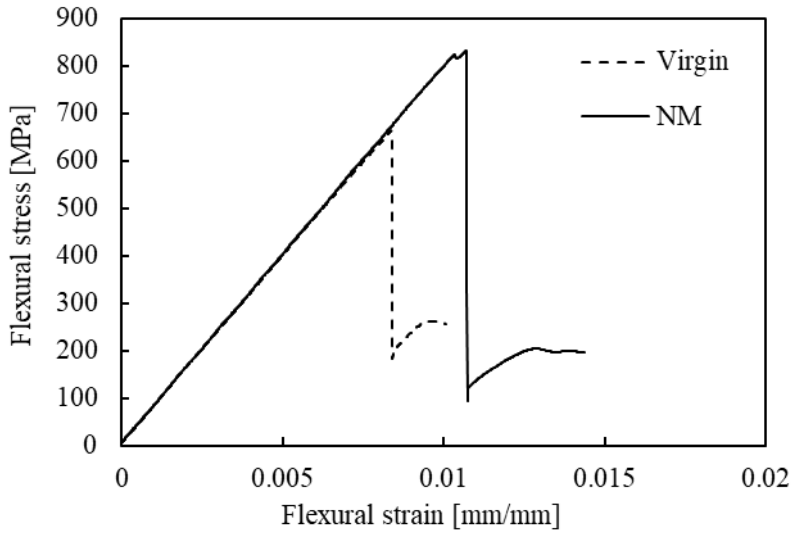

Fig. 6. Typical flexural stress-strain curve during the Flexural test of $[0/90]_s$ cross-ply laminates.

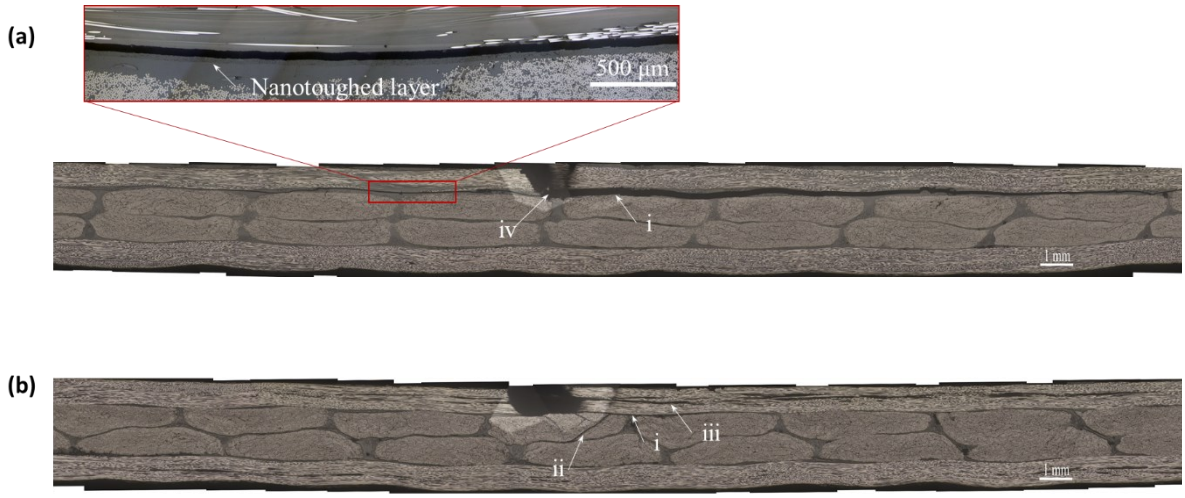

Fig. 7. Identification of failure modes for (a) $[0/90]_s$-nanomodified laminates and (b) $[0/90]_s$-virgin laminates in flexural tests; (I) interlamination delamination, (II) transverse interlaminar matrix crack, (III) intralaminar delamination.

2.4. Conclusion

Here, the conclusions of the experimental study for static flexural behavior of nanofiber interleaved cross-ply laminate system were summarised as follow:

- The ILSS was 37% higher in the NM configuration than virgin configuration, which was attributed to the improved shear properties of the matrix-rich region and high-strain plastic deformation within the nanofiber interlayer due to the reinforcement of the interlayer with the nanofiber veil.
- Although the NM configurations exhibit similar flexural modulus as the virgin configuration in the static 3-point flexural test, the UFS improvement was about 25.5%. The positive effect of nanofiber modified interlayer on energy absorption and load transfer was significant in lowering stress concentration, which was responsible for better UFS.

References

[18] Daelemans L, Van Der Heijden S, De Baere I, et al. Damage-Resistant Composites Using Electrospun Nanofibers: A Multiscale Analysis of the Toughening Mechanisms. ACS Appl Mater Interfaces. 2016;8:11806–11818.

[20] Beckermann GW, Pickering KL. Mode i and Mode II interlaminar fracture toughness of composite laminates interleaved with electrospun nanofibre veils. Compos Part A Appl Sci Manuf. 2015;72:11–21.

[26] Palazzetti R, Zucchelli A. Electrospun nanofibers as reinforcement for composite laminates materials – A review. Compos Struct [Internet]. 2017;182:711–727. Available from: https://doi.org/10.1016/j.compstruct.2017.09.021.

[45] Demircan O, Yilmaz C, Kocaman ES, et al. An experimental study on tensile and bending properties of biaxial warp knitted textile composites. Adv Compos Mater [Internet]. 2020;29:73–88. Available from: https://doi.org/10.1080/09243046.2019.1639016.

[46] Japanese Industrial Standards. Testing method of apparent interlaminar shear strength of carbon fiber reinforced plastics by three point loading method. Annu B JIS Stand.

[47] Akay M. Introduction to polymer science and technology. Bookboon; 2012.

[48] Kinloch AJ, Kodokian GKA, Watts JF. 44Relationships between the surface free energies and surface chemical compositions of thermoplastic fibre composites and adhesive joint strengths. J Mater Sci Lett. 1991;10:815–818.

[49] Zheng N, Liu HY, Gao J, et al. Synergetic improvement of interlaminar fracture energy in carbon fiber/epoxy composites with nylon nanofiber/polycaprolactone

blend interleaves. Compos Part B Eng. 2019;171:320–328.

[50] Kim JS, Lee SY, Roh JH. Failure analysis of laminated composites subjected to flexural loadings. Adv Compos Mater [Internet]. 2020;29:301–316. Available from: https://doi.org/10.1080/09243046.2020.1724467.

[51] Caminero MA, Rodríguez GP, Chacón JM, et al. Flexural damage response of symmetric cross-ply carbon fiber reinforced laminates: Effects of thickness and ply-scaling technique. Mech Adv Mater Struct [Internet]. 2021;28:212–219. Available from: https://doi.org/10.1080/15376494.2018.1553260.

[52] Beylergil B, Tanoğlu M, Aktaş E. Enhancement of interlaminar fracture toughness of carbon fiber–epoxy composites using polyamide-6,6 electrospun nanofibers. J Appl Polym Sci. 2017;134:1–12.

Chapter 3.

Experimental study on static flexural progressive damage behavior of nanofiber interlayered cross-ply non-crimp fabric composites.

3.1. Introduction

The effect of nanofiber interleaving on flexural progressive damage of cross-ply non-crimp fabric composites remains to be future discussed. To address this issue, two kinds of samples, virgin-$[0/90]_s$, nanomodified(NM)-$[0/90]_s$, were experimentally tested by the three-point bending method. Simultaneously the damage evolution behaviors were monitored by micrographic photos taken from the polished edge. Furthermore, the damage progress and failure mechanism were discussed.

3.2. Experiments

3.2.1. Material information

The materials using this study were the same as in chapter 2; these were described in section 2.2.1.

3.2.2. Composite preparation

The fabrication of the specimens was the same as chapter 2, the details of molding were explained in section 2.2.2.

3.2.3. Characterizations

The mechanical tests were conducted on TENSILON universal testing machine at a displacement-control velocity of 1 mm/min with two type of specimen: virgin-$[0/90]_s$, nanomodified(NM)-$[0/90]_s$. The specimen size and span space were the same as flexural bending test which is described in section 2.2.3. According to the mechanical behavior of cross-ply laminate composite, some key stress levels like 40%, 50%, 60%, 70%, 90%, 95% of ultimate flexural stress were selected to analyze the progressive

damage process, the test was interrupted at the stress level corresponding to these stress level, and the specimen was moved from the test machine to the OLYMPUS Microscope GX41 system for the edge scanning. After that, the sample was again moved back to the test machine and loaded to a higher stress level than the previous one, and its micrographic images were recorded. this process was repeated until the sample failure.

3.3. Result and discussion

The flexural stress-strain curves for static interrupted flexural test of virgin sample and NM sample were shown in Fig. 8(a) and (b), respectively. As shown in the static flexutal bending test in Chaper 2, the utimated flexural stress of NMsamples is 25% higher than that of the virgin sample due to the interlayer toughening effect of nanofibers.Thus .the felxural stress corresponding to each stress level of NM samples were higher than virgin samples finally the virgin sample and NM sample were failed at 644MPa (Fig. 8(a)) and 803.3 MPa(Fig. 8(b)), respectively, In addition, the curve trend of both configurations of samples for all stress levels demonstrated excellent repeatability, which means there was no apparent process of stiffness degradation before reaching the failure load under static flexural load for virgin and NM sample.

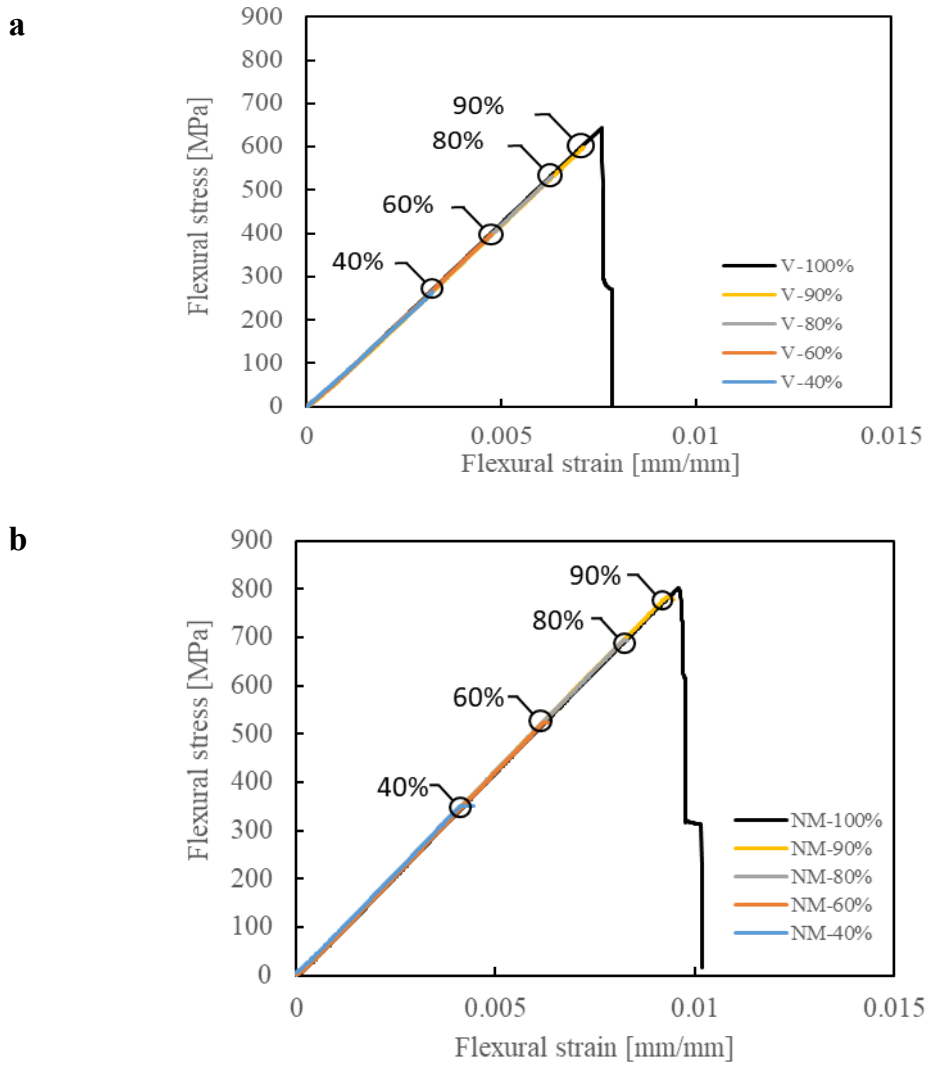

Fig. 8 Typical flexural stress-strain curve for static interrupted flexural test of virgin sample and NM sample.

Micrographic edge scanning was helpful to study the failure evolution of progressive damage at the microstructure level. The images obtained after the various stress level loading of NM specimen and virgin specimen were shownn in Fig. 9 and Fig. 10. In the 0%~90% state, no obvious damage was seen in interlayer or intralaminar for both configurations. This phenomenon well explained that there was no stiffness degradation before failure load under static bending load for specimen with or without nanofiber interleaving. However, it is undeniable that the high strain plastic deformation of the nanofiber toughened layer made the stress mainly concentrated in the nanotoughened

layer, which lead NM sample failing in form of interlayer delamination between 0°/90° layer. That was different from the failure mode of virgin sample in form of matrix cracking developed in the 90° ply.

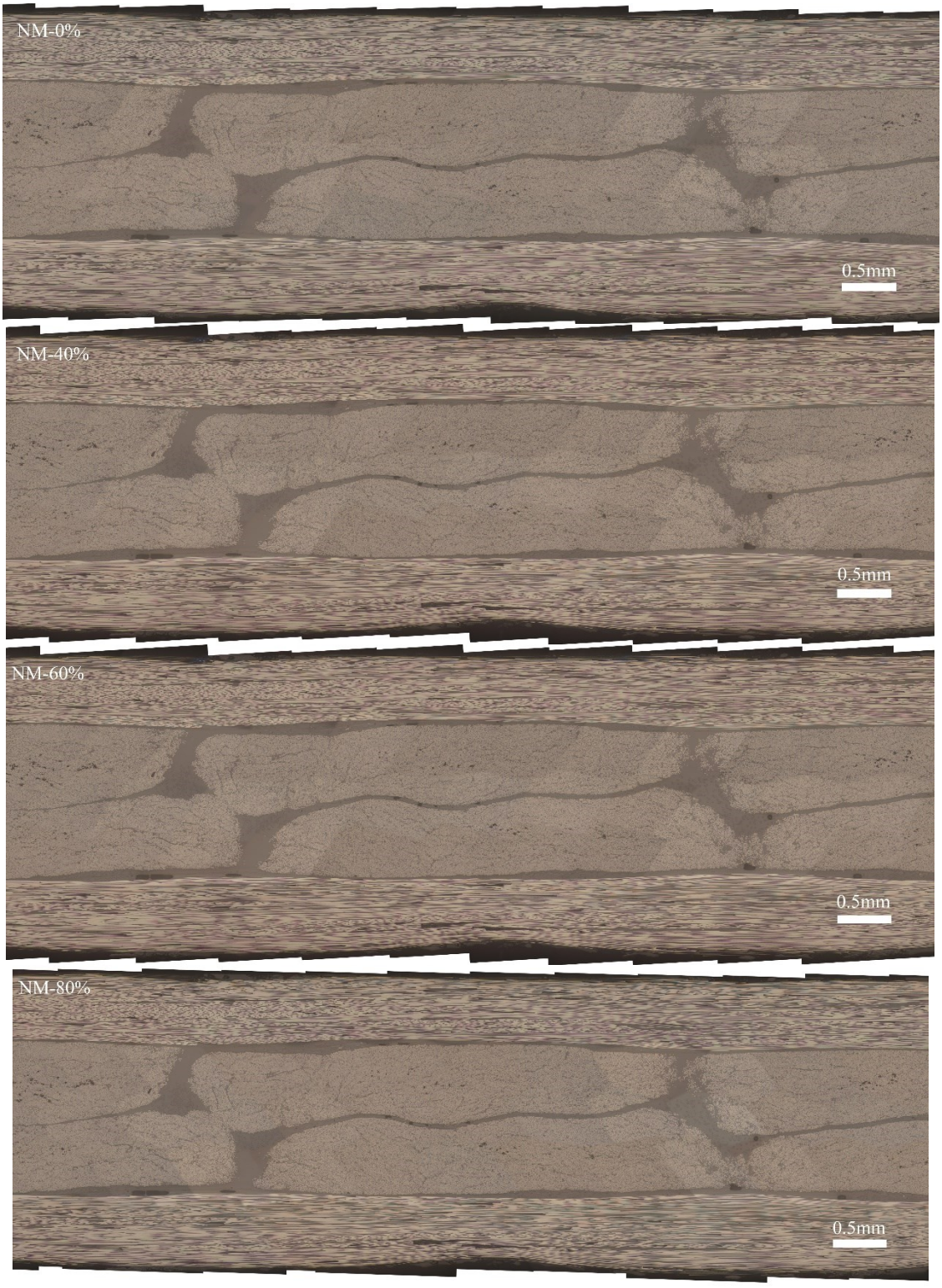

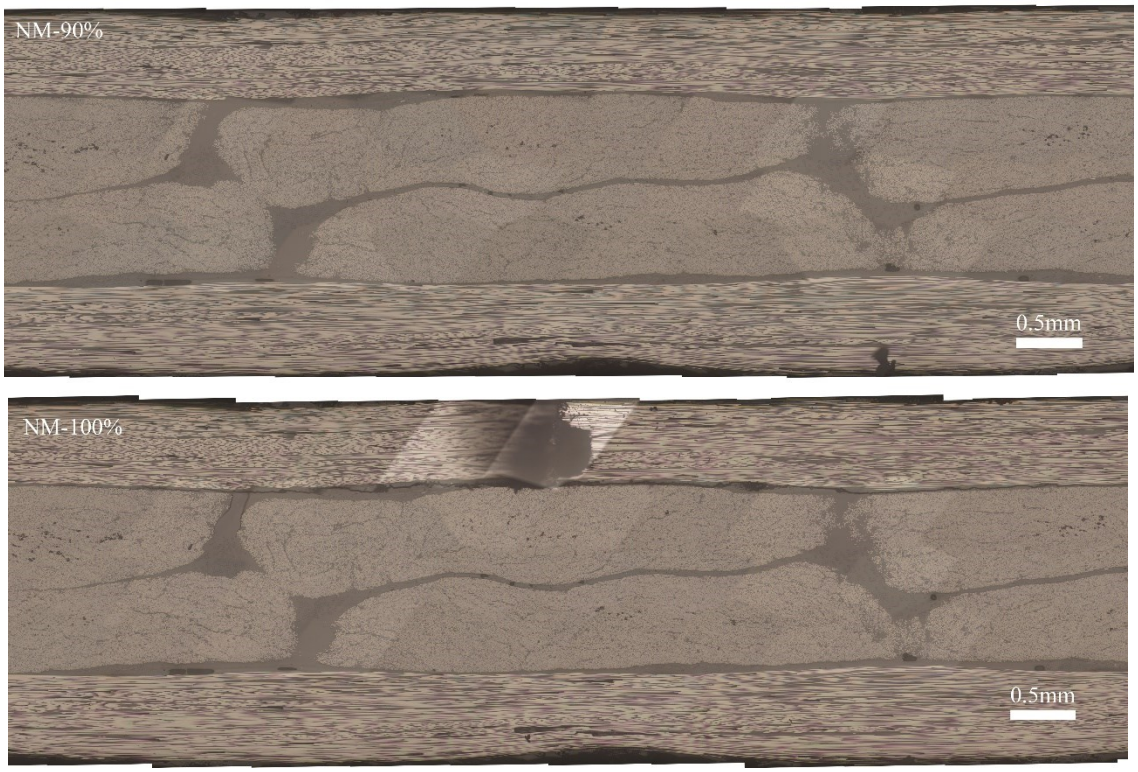

Fig. 9 Micrographic edge scanning of damage evolution corresponding to different loading stages on the load-displacement curve of the NM specimen.

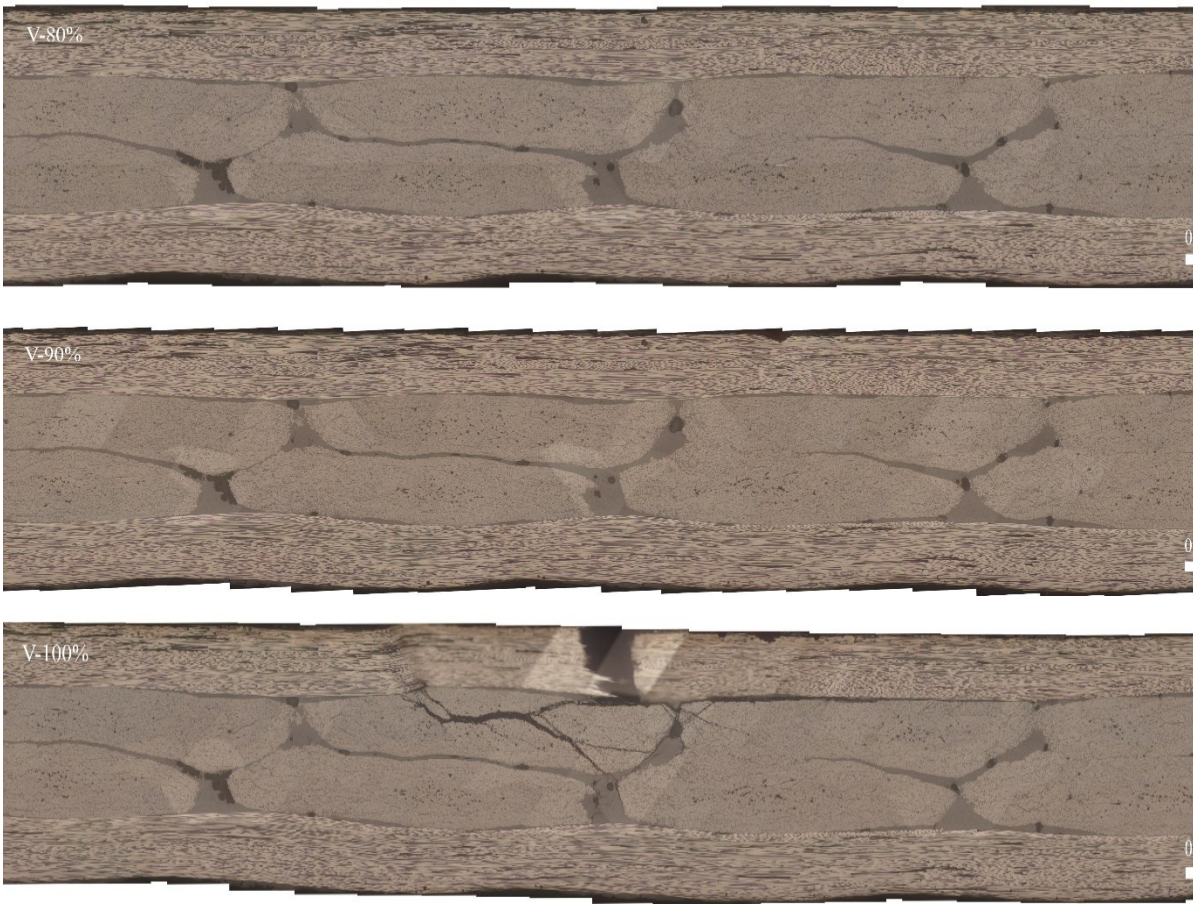

Fig. 10 Micrographic edge scanning of damage evolution corresponding to different loading stages on the load-displacement curve of the virgin specimen.

3.4. Conclusion

As a result of experimental study on the static flexutal progressive damage behavior behavior of nanofiber interlayered cross-ply non-crimp fabric composites, the following conclusions are drawn:

- The microscope system for the edge scanning was employed to investigate static felxural progressive damage behavior of nanofiber interlayered cross-ply non-crimp fabric composites.
- Both configurations (virgin and NM) did not exhibit the stiffness degradation behavior before structure failure.
- The micrographic images of the edge scanning showed that both configurations did not experience the damage before the failure stage.

- The failure mode of NM sample in form of interlayer delamination between 0°/90° layer was different from the failure mode of virgin sample in form of matrix cracking developed in the 90° ply.

Chapter 4.

Experimental study on flexural fatigue behavior of nanofiber interlayered cross-ply non-crimp fabric composites.

4.1. Introduction

In this chapter, the main objective was to investigate the effect of nanofiber interleaves on the fatigue behavior of the cross-ply CFRP laminate system. Two types of laminates, including virgin configuration and nanomodified configuration, were prepared for the test. The 3-point bending tests were carried out to evaluate the flexural fatigue behavior. Based on the viewpoint of stiffness degradation, the mechanisms of the contribution to the fatigue toughness by nanofiber veils were examined and discussed.

4.2. Experiments

4.2.1. Materials information

The materials using this study were same as in chapter 2; these were described in section 2.2.1.

4.2.2. Composite preparation

The fabrication of the specimens was the same as chapter 2, the details of molding were explained in section 2.2.2.

4.2.3. Characterizations

Two type of specimen: virgin-$[0/90]_s$, nanomodified(NM)-$[0/90]_s$ were prepared. The specimen size and span space were the same as flexural bending test which is described in section 2.2.3. Cyclic fatigue tests were conducted using a Shimadzu servo-hydraulic fatigue and endurance tester, working under the load-control mode and using a sinusoidal waveform. The test was conducted under standard laboratory conditions at

a frequency of 2 Hz and an R value of 0.25 (R is the ratio of minimum to maximum cyclic load). Maximum stress values of 40% to 90% of the ultimate flexural stress (UFS) were applied in both laminate types, and three tests were performed at each stress level. The instrument was set to stop when a loading pin of more than 10 mm on defection was detected, enabling specimens to be completely broken before the instrument stopped and preventing the load pin from loading impact onto the supports. The load-deflection data was obtained using a computer.

4.3. Result and discussion

Generally, because the composite materials exhibit the anisotropic characteristics in mechanical behavior, the fatigue behavior of composite is more complicated than metals. As a matter of fact, it is precisely because the anisotropic and heterogeneous nature of the composite causes the formation of different stress levels within the material. Consequently, compared with the metal fatigue damage due to a single main crack, the fatigue damage of the composite shows material degradation behavior caused by damage accumulation in the entire volume. Meanwhile, micro-crack initiated at the early stage of fatigue damage of composite will not affect the endurance of the material[53].

The authors initially adopted two main approaches to assess the fatigue life and material degradation behavior of composite material. One approach was the displacement-controlled tests, which scale the degradation rate of stiffness according to the stress level within the composite sample under constant amplitude deflection cycling; the other one was the load-controlled tests, which constantly use the deflection level to scale the degradation rate of stiffness under constant amplitude load cycling.

As reported in [54], similar results were obtained from both loading conditions. For our study, all tests were conducted with the load control condition.

Fig. 11 plotted the relationship between bending deflection and the number of cycles at each load stress levels, the minus sign here represent the deflection direction is downward relative to the horizontal 0 axis,the results exhibited that all specimens exhibit progressive damage in laminate as a similar experimental study reported in papers [54–58]. A high percentage stress level caused structural failure at low cyclical life for virgin configurations easily. . However, for NM samples, the deflection increases slightly with an increase in load cycles under high stress, but no specimen failure occurred. Moreover, since the flexural modulus of NM laminates was identical with virgin laminates and the UFS was 25.5% higher than virgin ones (Table 2), the deflection of NM samples was higher than virgin samples under the same stress level. These phenomena indicated that nanofibers have a positive effect on enhancing the interlayer toughness and maintaining the overall stiffness of the NM laminate during cycling load.

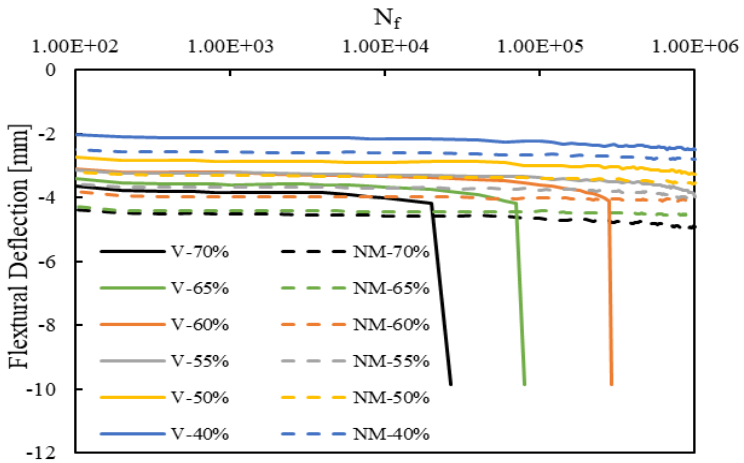

Fig. 11. Increment of bending deflection through 10^6 cycles vs number of cycles. Curves are plotting in different percentages of the UFS (40%~70%).

In order to achieve a better understanding of how the nanofiber interleaves respond to the fatigue stiffness of laminate, the stiffness degradation was evaluated. i.e., the specimen subject constant amplitude load cycling condition, in the primary stage, constant load build up less deflection; as cycling increases, the internal damage material needs large deflection to produce resistance stress. These deflection changes were used to detect the stiffness change of the specimen. As often presented in the paper for similar experimental studies[55,56], for the sake of quantifying the amount of degradation of stiffness during a bending fatigue test, the relative flexural stiffness(RFS) was introduced. This parameter is defined as the ratio of the flexural modulus measured in N^{th} cycle to the flexural modulus measured in the first cycle. The flexural modulus is calculated by using the following equation:

$$E_{nr} = \frac{W_{max} L^3}{4bh^3 e_n}$$

where E_{nr} is the flexural modulus at some load cycle, n, and stress level, r; W_{max} is the maximum load; e_n is the deflection corresponding to the maximum load at the N^{th} cycle. The validity of this equation was proven by the work of M. Buggy and G. Dillon [58].

Fig. 12 shows the variation in RFS with an increased cycle count plot for different stress levels. The data indicated that the distinct different behavior was presented in configurations which with nanofiber or without nanofibr. The semi-logarithmic graph of virgin samples showed that the virgin configuration retains the initial stiffness almost before 1E+03 cyclesand then, the stiffness decrease in proportion to the logarithm of cycles until approaching failure (Fig. 12 a). For the NM samples (Fig. 12 b), the initial

stiffness state was maintained until the 1E+4 cycles and then, a slight decrease was observed until approaching failure.

Notably, the maximum stiffness reduction of the virgin configuration was about 21%, but the NM sample was about 10%, which can be because the NM configuration did not experience extensive matrix damage and microcracks after 10E+6 cycles of fatigue loading (Fig. 13), which was attributed to the nanofiber-toughened layer that distributes more stress and transmits the load toward the carbon fibers to absorb more energy.

(a)

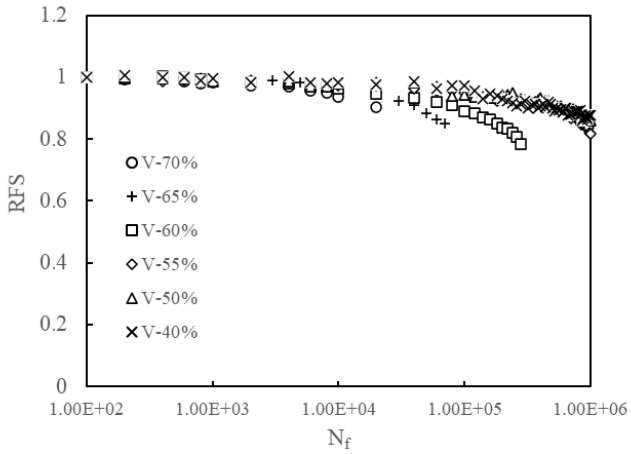

(b)

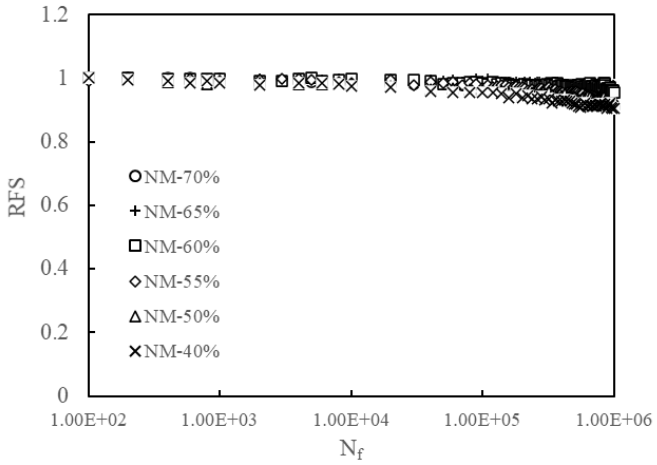

Fig. 12. The curves of relative flexural stiffness through 106 cycles versus the number of cycles are plotting in different percentages of the UFS (40%~70%). (a) virgin composite (b) nanofiber modified composite.

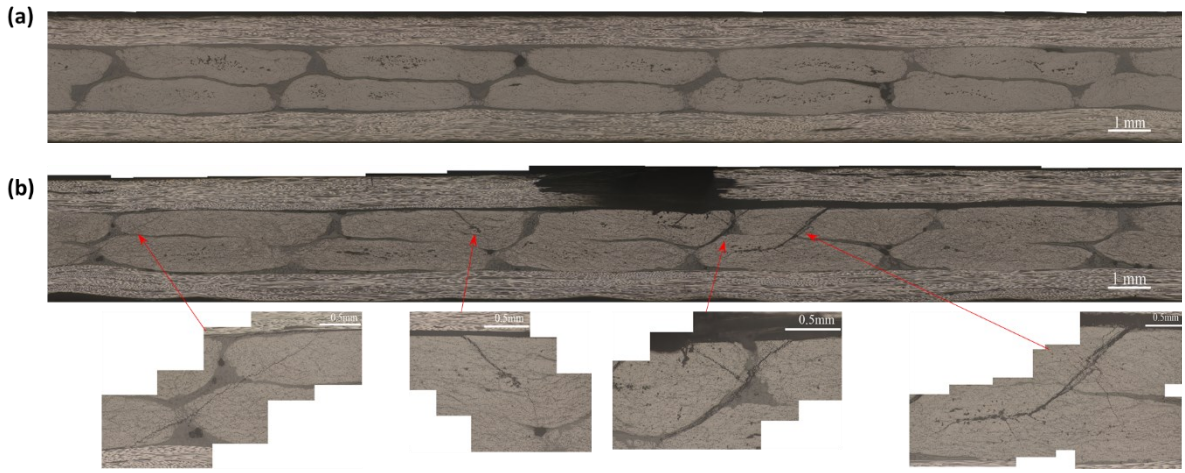

Fig. 13 Damage observation of fatigue test run at 60% UFS. (a) the nanofiber modified composite run-out of 106 cycles (b) the failure of virgin composite.

By plotting the relationship between RFS and the number of cycles on the semi-logarithmic scale, the reduction in stiffness may be observed to be linear with the logarithm of the number of cycles. Fig. 14 reported data for a fatigue test performed at 60% UFS on a virgin specimen. A linear relationship allowed a good fit between RFS and the number of cycles on the semi-logarithmic scale. And the Equation obtained by linear regression was reported in the figure. Thus, the stiffness decrease rates for other stress levels were obtained in a similar procedure (Fig. 15). At low-stress levels (up to 50%), both configurations exhibited a similar decrease rate in stiffness, but from 60% on, the absolute value of stiffness decrease rate of the NM samples was significantly lower than the virgin samples, demonstrating that the interleaved reinforcement by nanofiber veils had a remarkable effect that enables the maintenance of the laminate stiffness during the fatigue life.

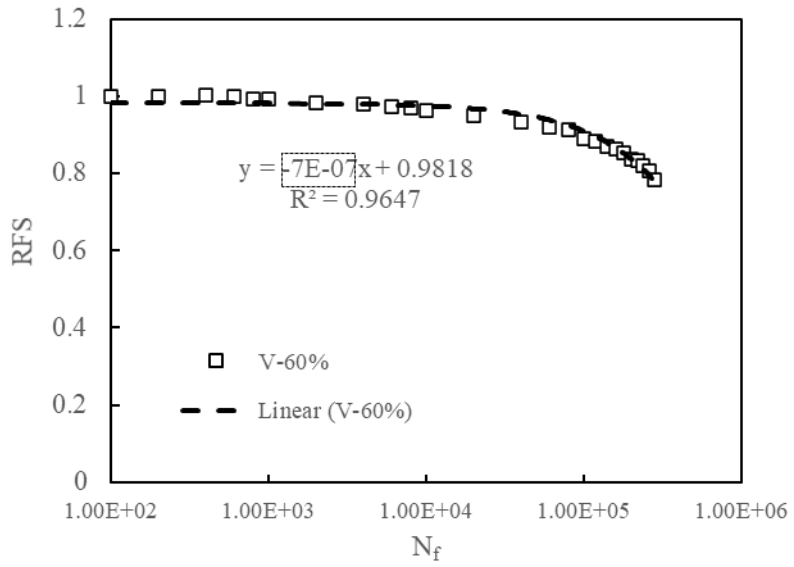

Fig. 14. Loss of stiffness through 106 cycles vs the number of cycles. Data are for a fatigue test run at 60% UFS on a virgin specimen.

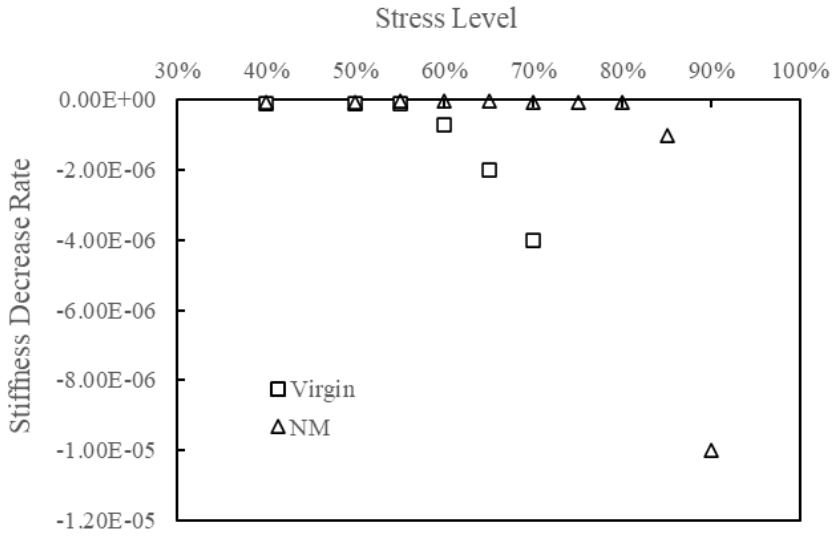

Fig. 15. Stiffness decrease rate against stress level.

The results of the fatigue tests were plotted in terms of stress range versus the number of cycles to failureas shown in Fig. 16(a), the results indicates that the fatigue strength of the NM sample (624,6MPa) was 1.7 times higher than the virgin configurations (365.2MPa). This effect was attributed to two aspects; first, the nanofibers could transfer the load toward the carbon fibers to reduce the stress concentration; second, the

nanofiber interlayer performed similarly thermoplastic particle interlayers [8,9], effectively transferring the ductile behavior of the thermoplastic-rich phase to the interlayer to enhance energy absorption behavior. In addition, some vital information concerning run-out data points in accordance with fatigue results in terms of the normalized strength range (Flexural strength/UFS) against the number of cycles to failure (see in Fig. 16 (b)) was worth highlighting. The fatigue loading applied to the virgin specimens at almost 55% of UFS had not yet achieved failure after 10^6 cycles, whereas the run-out point for NM samples was 75% of UFS. In other words, the NM configuration could provide far-ranging of allowable fatigue stress intensity and an excellent capability of fatigue energy absorption of deflection, for the composite configuration designer since the NM configuration could withstand high fatigue load and high deflection deformation.

Finally, considering the influence of the fatigue load on the residual strength of the precycling specimen, the relationship between the normalized residual strength, defined as residual strength/UFS versus fatigue stress level, was plotted in Fig. 17. Although both configurations exhibited a similar trend, the residual strength decreased with an increase in fatigue load level as anticipated. The stiffness reduction could not accurately predict the residual strength because the maximum reduction of RFS of the precycled NM samples was 10%, as reported above, but the reduction in maximum residual strength was about 26%.

(a)

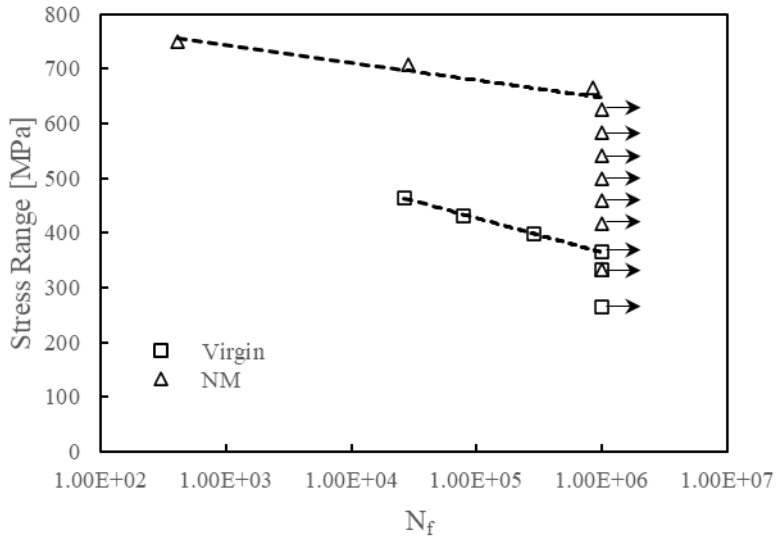

(b)

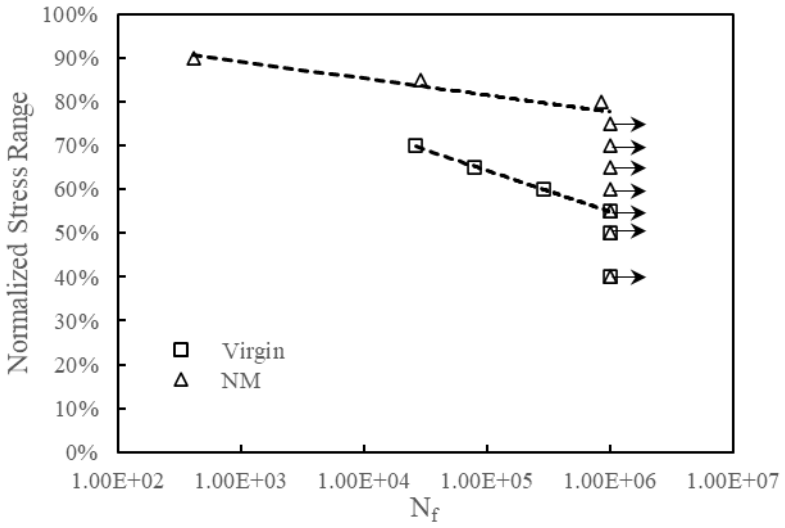

Fig. 16. Traditional fatigue results of NM configuration and virgin configuration in (a)stress range scale and (b)normalized stress range.

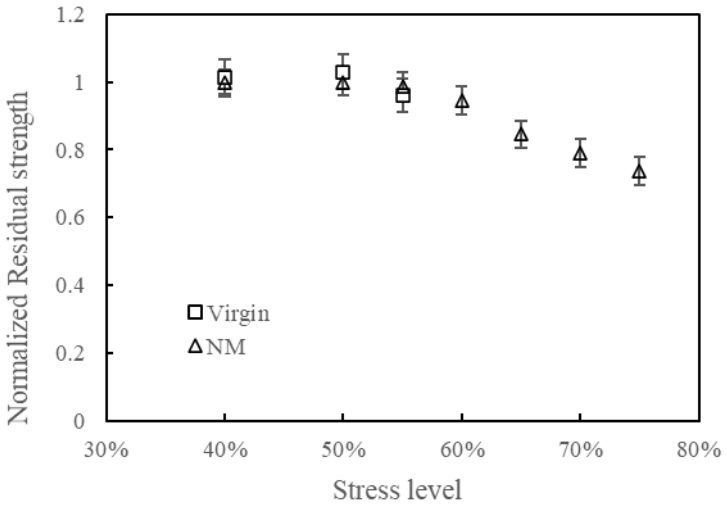

Fig. 17. Normalized residual strength versus stress level for virgin and NM configuration.

4.4. Conclusion

As a result of evaluating the study for the effect of nanofiber interleaves on fatigue behavior of cross-ply CFRP laminate system, the following conclusions are drawn:

- All composite specimens showed progressive damage under the load-control fatigue test. Because the NM configuration had a higher UFS and identical elastic modulus with the virgin configuration, a higher deflection was observed under the same percentage levels, implying that nanofiber interleaves effectively enhanced the toughness and stiffness holding of the laminate.
- The description of progressive damage was evaluated by measuring the increment of deflection expressed by the RFS parameter. The information on the stiffness reduction was extracted from the plot of RFS versus the number of cycles and used to compare the configurations. The NM configuration exhibited the best initial stiffness retention, with a maximum stiffness reduction of about 10% compared with 21% for the virgin configuration. It was considered to be

that the nanofiber-toughened layer could distribute more stress and transmit the load toward the carbon fibers to absorb more energy.

- Analyzing the stiffness decrease rate showed that the value of NM samples was significantly lower than the virgin sample, indicating that the nanofiber interleaves had a strong affinity for retaining the stiffness of laminate during the fatigue life.
- The traditional S-N plotting revealed that the fatigue strength of the NM configuration was 1.7 times higher than the virgin configuration. Run-out point analysis illustrated the NM configuration presented the higher percentage stress level with UFS, which continued to be a great impetus to research efforts to enhance the material's fatigue stress level and optimize its fatigue energy absorption capacity.
- The residual strength investigation revealed that the higher fatigue loading resulted in more material damage and lower residual strength. However, the reduction of the residual stress was independent of the stiffness reduction.

References

[8] Hojo M, Matsuda S, Tanaka M, et al. Mode I delamination fatigue properties of interlayer-toughened CF/epoxy laminates. Compos Sci Technol. 2006;66:665–675.

[9] Gao F, Jiao G, Lu Z, et al. Mode II delamination and damage resistance of carbon/epoxy composite laminates interleaved with thermoplastic particles. J Compos Mater. 2007;41:111–123.

[53] Nairn JA. Microcracking, Microcrack-Induced Delamination, and Longitudinal Splitting of Advanced Composite Structures. NASA Contract. Rep. 4472. 1992;P144.

[54] Ferreira JAM, Costa JDM, Reis PNB, et al. Analysis of fatigue and damage in glass-fibre-reinforced polypropylene composite materials. Compos Sci Technol. 1999;59:1461–1467.

[55] Belingardi G, Cavatorta MP, Frasca C. Bending fatigue behavior of glass-carbon/epoxy hybrid composites. Compos Sci Technol. 2006;66:222–232.

[56] Belingardi G, Cavatorta MP. Bending fatigue stiffness and strength degradation in carbon-glass/epoxy hybrid laminates: Cross-ply vs. angle-ply specimens. Int J Fatigue. 2006;28:815–825.

[57] Reis PNB, Ferreira JAM, Antunes F V., et al. Flexural behaviour of hybrid laminated composites. Compos Part A Appl Sci Manuf. 2007;38:1612–1620.

[58] M. BUGGY， G.DILLON. Flexural fatigue of carbon fibre-reinforced PEEK laminates. COMPOSITES. 1991;22:191–198.

Chapter 5.

Experimental study on static flexural behavior of nanofiber interleaved CFRTP composites

5.1. Introduction

In previous studies, the authors paid more attention to the application of electrospun nanofiber in strengthening the interlaminar of thermosetting resin-based composite laminate, whereas the thermoplastic resin-based composites laminate are more and more widely used since they possess characteristics of high-production efficiency and recyclability. Therefore, The PA electrospun nanofiber was chosen as the interleaf material, and the main objective in this chaper was to investigate the influence of the nanofiber interleaf on the static flexural mechanical properties of non-crimp fabric lay-up laminate based on the thermoplastic resin (PMMA) by static flexural tests. The laminate systems, including virgin configuration and nanomodified configuration, could be fabricated by the thermo-compression technique.

5.2. Experiments

5.2.1. Prepreg sheet preparation

The prepreg sheets of the CFRTP consist of non-crimped carbon fabrics (NCFs) and copolymer, with NCFs used as a reinforcing material and copolymer used as a matrix resin. The NCFs were provided by Hokuriku fiberglass Co., Ltd, which fabric by using T700-24K from Toray Inc stitched into a unidirectional 0° NCF fabric of 793 g/mm2. The polymers composed of MMA (FUJIFILM Wako Pure Chemical Corp.) were synthesized by the free-radical bulk polymerization, then 2,2'-Azobis(2,4-dimethylvaleronitrile) (FUJIFILM Wako Pure Chemical Corp.) of 0.5 w/w% was used as an initiator. The prepreg sheets were prepared according to the following procedure,

as shown in Fig. 18. These mixed monomer liquids were poured into an the easy-removable fluorinated rubber mold (Perfluoroalkoxy polymer (PFA resin) on which a sheet of NCF was placed. Subsequently, the liquids were well impregnated to the NCF. Next,the bulk polymerizations were carried out at 60℃ for 2 hrs in the mold. After that, the processes were completed via second heating at 100℃ for 12 hrs, and 130℃ for 5 hrs. The thickness of the prepreg sheet obtained was about 0.9 mm.

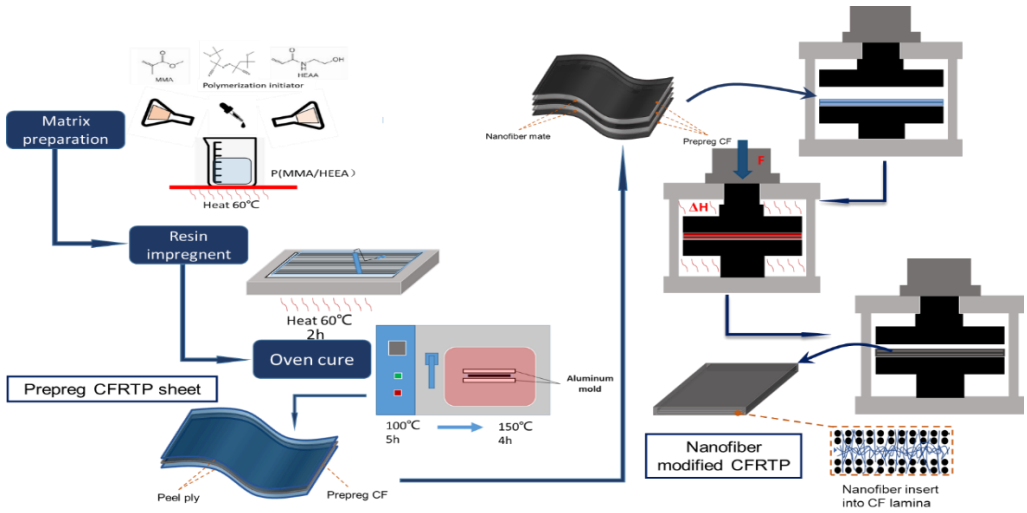

Fig. 18. Schematic view of the production route used to obtain nanofiber modified CFRTP specimens.

The Vf of prepreg was measured by weight loss measurements using a Thermogravimetric Analyzer (TGA). The specimen was cut from the prepreg sheet into fine particles. And the test weight of the specimen was approximately 20 mg suitable. The heating program developed for the composite consists of heating from room temperature to 500 ℃ at 20 ℃/min heating rate and then kept at 500 ℃ for 60 min which ensures enough weight loss of resin, followed by heating at 10 ℃/min to 1000 ℃ and then kept at 1000 ℃ for 20 min which ensures enough weight loss of carbon fiber. A typical weight loss curve is shown in Fig. 19. The results showed that the Vf of the obtained prepreg sheet obtained was about 48%.

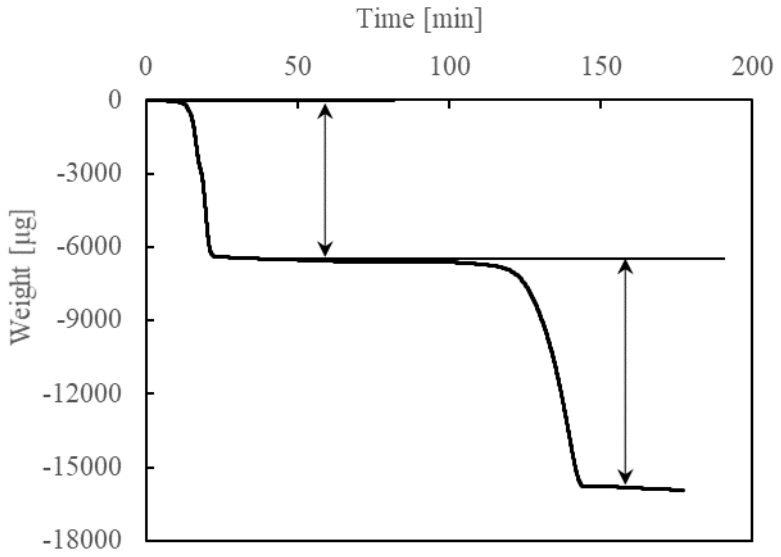

Fig. 19 Weight function of time for NCF/PMMA prepreg composite.

5.2.2. Fabrication of CFRTP laminate

CFRTP cross-ply composites were produced by the thermo-compression technique. The nano-modified (NM) composite panels and virgin with four piles of prepreg sheet in a $[0/90]_s$ orientation were prepared in which the nanofiber veils were inserted in each interface between 0°- and 90°- oriented plies for nanofiber interleaved plates, then the prepreg layup was transferred into a thermo-compressor at 185 ℃ and 0.4 MPa to allow complete melting of the PMMA into the continuous matrix phase, within which the nanofibrous morphology of the nanofiber remained as the reinforcement phase (nanofiber melt point is about 186 ℃ which determined by DSC showed in Fig. 20). After 20 min,the pressure was then increased to 4 MPa and kept for 20 min. Afterward, the pressure was removed, and the mold was cooled to ambient temperature. Fig. 21 shows the cross-sectional micrograph of cross-ply laminate with nanofiber and without nanofiber. which can confirm that the nanofiber reinforced interlayer existed between 0° and 90° layer in NM samples. Here, electrospun nanofiber veils, called Xantu.Layr XLB, were supplied by Revolution Fibres Ltd (Auckland, New Zealand), which had an

areal density of 4 g/m^2. The composition of nanofibers was PA-XD10 produced by Mitsubishi Gas Chemical Inc (Tokyo, Japan).

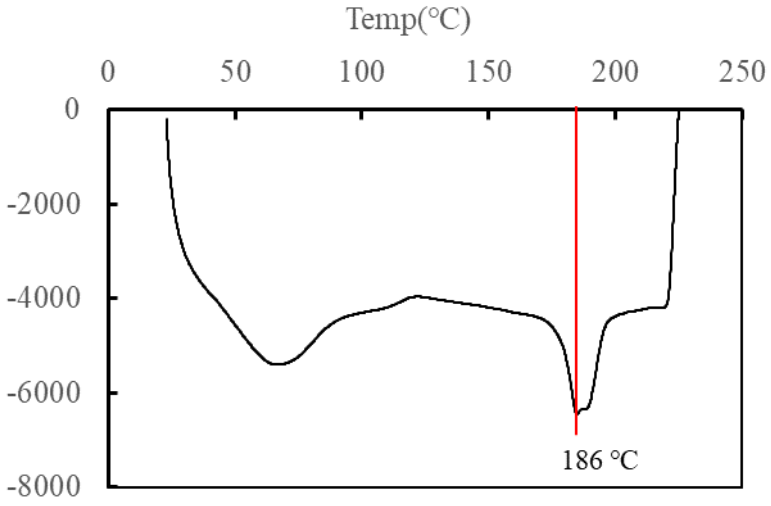

Fig. 20 DSC analysis of thermoplastic polymer nanofiber

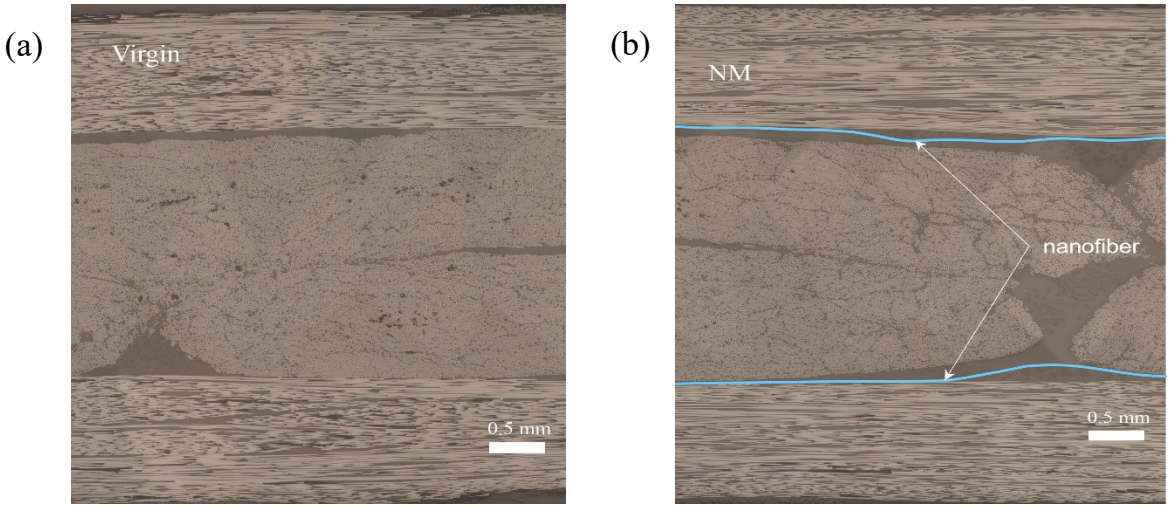

Fig. 21 Micrograph of cross-ply CFRTP laminate structure in cross-section. (a) virgin composite (b) nanofiber modified composite.

5.2.3. Characterizations

The characterization of the specimens was the same as chapter 2, the detail of 3-point bending test was explained in section 2.2.3.

5.3. Result and discussion

A series of three-point bending tests were conducted on the virgin and NM samples to investigate the interlaminar reinforcement effect of nanofiber veil on the flexural properties and their bulk failure mode. Fig. 22 presented the typical flexural stress-strain curves of virgin and NM samples, the results indicated that the stress increases linearly as the strain increases for both configurations at initial stage. After reached the maximum critical stress, the NM samples exhibited brittle fracture behavior, whereas the stress for the virgin samples exhibited the ladder down trend. The flexural modulus and ultimate flexural stress (UFS) of cross-ply CFRTP were sumerised in Table 3. The result indicated that the nanofiber interleaving made a good improvement in ultimate flexural modulus and UFS of cross-ply CFRTP laminate about 12.5% and 44.8% respectively, comparing with virgin samples. This phenomenon preliminarily indicates that the nanofiber layer can inhibit the premature formation of cracks in the CFRTP laminating system, and improve the flexural behavior of the thermoplastic laminating system. Therefore, in the subsequent chapters, the interlaminar fracture behavior of the thermoplastic laminated system toughened by nanofibers will be discussed in detail.

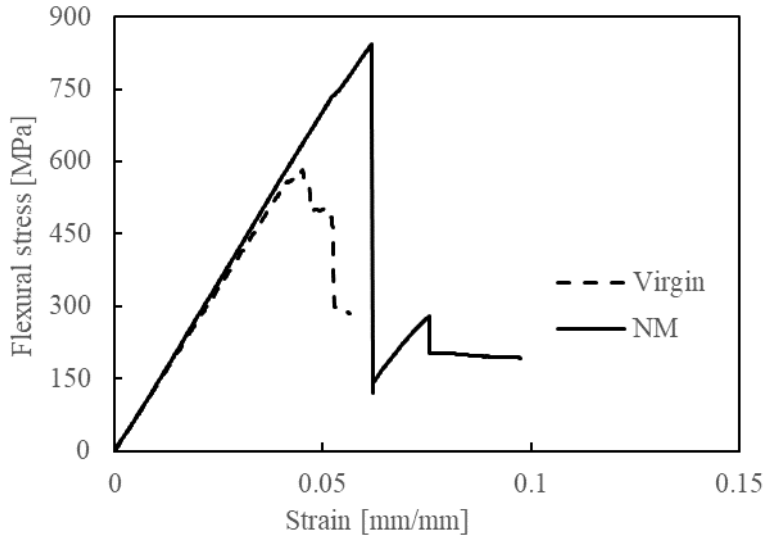

Fig. 22 Typical flexural stress-strain curve during the Flexural test of $[0/90]_s$ cross-ply CFRTP laminates.

Table 3. The flexural properties of different CFRTP laminates.

Lay-up		σ_f[MPa]	E_f[GPa]
$[0/90]_s$	-virgin	581.7	68.5
	-NM	842.4	77.1

5.4. Conclusion

As a result of experimental studies on the effects of nanofiber interleaves on the static flexural behavior of cross-ply CFRTP laminate system, the following conclusions were drawn:

- The results of static flexural behavior showed that nanofiber interleaving had great potential in toughing the CFRTP system.

Chapter 6.

Experimental study on Mode-I fracture behavior of nanofiber interleaved CFRTP composites

6.1. Introduction

In the previous chapter, the static flexural tests shows that the interlaminar toughening of nanofibers has good strengthening effect on the flexural behavior of CFRTP laminated system and better inhibits the premature initiation of interlaminar cracks. Thus, the main objective in this chapter was to investigate the mechanisms of Mode-I interlaminar toughness for nanofiber interleaved CFRTP laminate composites. The PA electrospun nanofiber was chosen as the interleaf material. Furthermore, the compatibility of PMMA resin is typically poor with PA nanofibers and CF fiber. While interfacial adhesion of polymer to CF and nanofiber is the key to realize the potential of interlayer toughing effect of PA nanofiber. Based on the previous research experience[59], the functional monomer hydroxyethyl acrylamide (HEAA) for copolymerization with methyl methacrylate (MMA) was chosen as the modified thermoplastic resin to improve fiber/resin interfacial adhesion. The CFRTP laminate system interleaved with/without nanofiber could be made by the hot-press technique under reasonable hot-press conditions. The Mode-I interlaminar toughness was examined by double-cantilever beam (DCB) tests. The fracture surface of tested specimens was observed using the scanning electron microscope (SEM). The effects of modified resin copolymerized with different molar concentrations of HEAA on the Mode-I toughness enhancement of nanofiber interleaves was discussed, combined with the test results of the SEM observation.

6.2. Experiments

6.2.1. Prepreg sheet preparation

The prepreg sheets of the CFRTP consist of non-crimped carbon fabrics (NCFs) and copolymer, with NCFs used as a reinforcing material and copolymer used as a matrix resin. The NCFs were provided by Hokuriku fiberglass Co., Ltd, which fabric by using T700-24K from Toray Inc stitched into a unidirectional 0° NCF fabric of 793 g/mm2. The copolymers composed of MMA (FUJIFILM Wako Pure Chemical Corp.) and HEAA (TCI Co., Ltd.) were synthesized by the free-radical bulk polymerization, then 2,2'-Azobis(2,4-dimethylvaleronitrile) (FUJIFILM Wako Pure Chemical Corp.) of 0.5 w/w% was used as an initiator. The prepared feeds (molar ratios) of MMA/HEAA were 100/0, 99/1, 97/3, and 95/5, respectively. The prepreg sheets were prepared according to the following procedure. These mixed monomer liquids were poured into an easy-removable fluorinated rubber mold (Perfluoroalkoxy polymer (PFA resin) on which a sheet of NCF was placed. Subsequently, the liquids were well impregnated to the NCF. Next, the bulk polymerizations were carried out at 60℃ for 2 hrs in the mold. After that, the processes were completed via second heating at 100℃ for 12 hrs, and 130℃ for 5 hrs. The thickness and Vf of the prepreg sheet obtained were about 0.9 mm and 48%, respectively. These copolymer compositions are listed in Table 4, The observed compositions of the HEAA unit in the copolymer were concentrated during the reaction process, This was due to the evaporation of another MMA monomer liquid at the initial stage of polymerization under heating, resulting in a decrease in the compositions of the MMA unit in the copolymer.

Table 4. Properties of copolymer.

Copolymer	Feed of HEAA	Composition of HEAA*	E^*	S_{max}**
	[mol%]	[mol%]	[GPa]	[MPa]
PMMA	0	0	1.62	25.5
PMMA/HEAA1	1	3.5±1.0	1.54	32.3
PMMA/HEAA3	3	5.7±0.7	1.32	37.1
PMMA/HEAA5	5	7.5±1.5	1.22	31.1

*Determined by proton NMR
** Young's modulus of matrix resin
*** Maximum stress of matrix

In addition, the tensile tests were performed to examine the mechanical properties of copolymers as the matrix with the form of a 40 mm × 10 mm × 0.3~0.5 mm (length × width × thickness) rectangular strip shape, gage length was 20 mm. The samples were extended at 0.2 mm/min, and the typical stress-strain curve was extracted from the load-displacement data obtained from the tool shown in Fig. 23. Young's modulus was obtained from the initial slope of the stress-strain curve. The results indicated that the nonlinear fracture behavior of the copolymers gradually changed from brittle fracture to yield plastic fracture, and the linear behavior also gradually exhibited softening characteristics with the increase in the HEAA component. The composition of HEAA and mechanical property of each copolymer are summarized in Table 4.

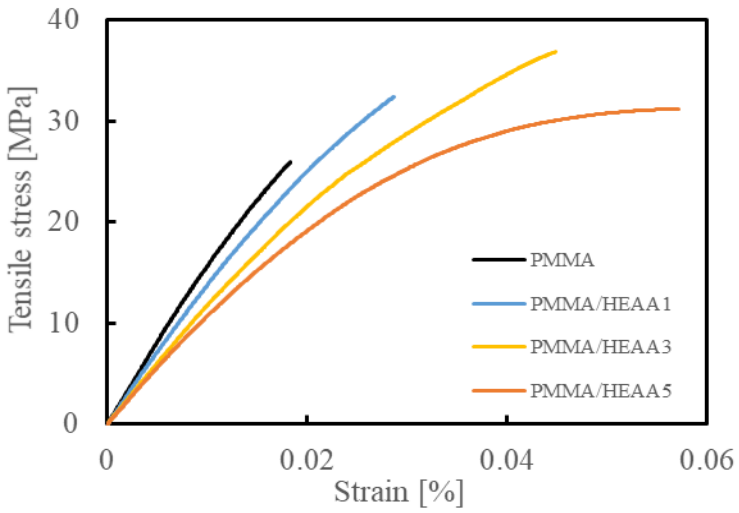

Fig. 23 Typical tensile stress-strain curves for copolymers used as matrix for CFRP composite.

6.2.2. Fabrication of CFRTP laminate

The nano-modified composite and the virgin panels with four piles of prepreg sheet in the 0° orientation were prepared according to the method described in the JIS K 7086 standard [60]. A stainless film (0.015mm thick) was inserted in the middle-plane at the tip of the panel to form a 40 mm initial artificial crack. Besides, the nanofiber veils were needed to place at the end of the stainless film at the same time to form a nano-modified interlayer for the nano-modified composite. The prepreg layup was transferred into a thermo-compressor at 185 ℃ and 0.4 MPa to melt the matrix. After 20 min, the pressure was then increased to 4 MPa and kept for 20 min. Afterward, the pressure was removed, and the mold was cooled to ambient temperature. Fig. 24 shows that the cross-sectional micrograph of specimens with nanofiber and without nanofiber. It can be found that the effect of nanofiber veil as the nano reinforcing material inserted into the interlayer on the thickness of the final production can be negligible due to its ultra thin-film characteristics (sample with nanofiber: 3.3mm, sample without nanofiber:3.2 mm). And the Vf of nano-modified sample and virgin samples was 50.3%, 51.5%, respectively. Here, electrospun nanofiber veils, called Xantu.Layr XLB, were supplied by Revolution Fibres Ltd (Auckland, New Zealand), which had an areal density of 4 g/m^2. The composition of nanofibers was PA-XD10 produced by Mitsubishi Gas Chemical Inc (Tokyo, Japan).

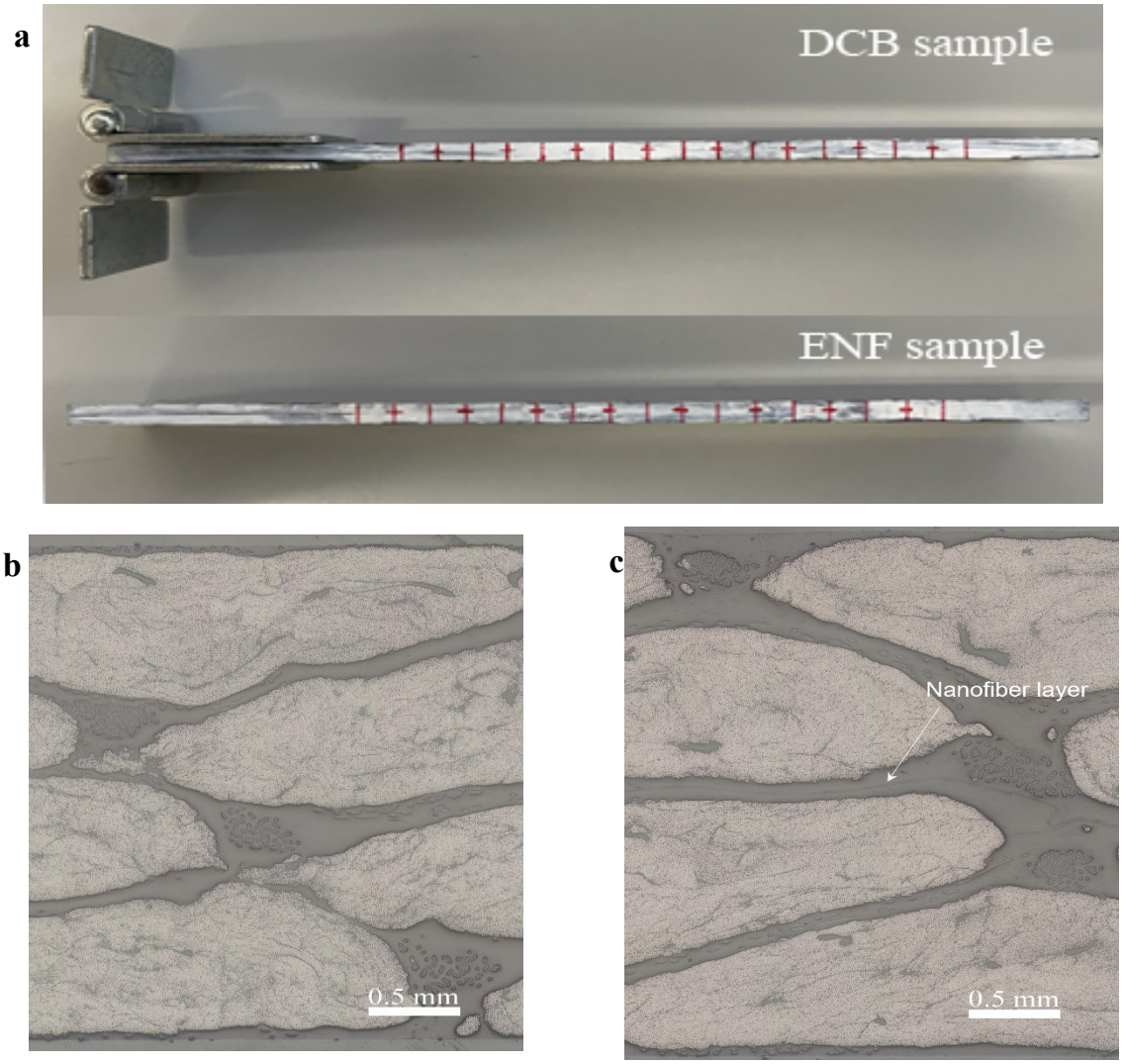

Fig. 24 Photograph of DCB and ENF sample (a) and micrograph of specimens with nanofiber (c) without nanofiber (b) in cross-section.

6.2.3. Characterization

To investigate the delamination of material in an opening mode of failure (Mode-I), the double cantilever beam (DCB) test was performed according to standard JIS K 7086 for carbon fiber reinforced plastics [61] using a universal test machine equipped with a 50 kN load cell in 1% load range. The geometry of the specimens was L=140mm in length and b=20 mm in width. Piano hinges were bonded to the outer surface of the specimens to apply the opening forces. The tests were carried out at a constant crosshead speed of 0.5 mm/min. During the test, the load-displacement data was recorded, and a

traveling microscope equipped with a displacement recorder, was employed to measure the progressive crack length by focusing on the edge of the DCB specimen. The fracture toughness of DCB tests was calculated using a modified beam theory (MBT), as follows:

$$G_I = \frac{3}{2(2H)} \frac{P}{B} \frac{(B\lambda)^{\frac{2}{3}}}{\alpha_1}$$

where H, B, P, λ are the specimen thickness, width, the load applied, compliance which is determined by the ratio of displacement to load, respectively. α_1 is determined experimentally by generating a least-square plot of the cube root of Bλ, as a function of a/2H.

To get a better handle on the Mode-I results, two stages of crack propagation was divided: the initiation stage, which was delamination onset from the artificial crack (critical energy release rate, G_{IC}), and the propagation stage determined the crack between 60mm and 100mm of length (propagation energy release rate, G_{IR}).

All specimens were cut from the composite panel obtained above using a water-cooled diamond cutting machine. A total of 6 different configurations were tested as summarized in Table 5., in which the original sample was marked as "V," and the nano-modified sample was marked as "NFR". For each configuration, at least three copies have been tested.

Hitachi S-4700 field emission scanning electron microscope was employed to inspect and image the fractured surface of the sample. The samples were plasma-coated with osmium for 10 s.

Table 5. Nomenclature of CFRTP specimens used for mechanical tests.

Specimen	Matrix	Nanofiber	Fiber
V0	PMMA	No	NCF
NFR0	PMMA	Yes	NCF
NFR1	PMMA/HEAA1	Yes	NCF
NFR3	PMMA/HEAA3	Yes	NCF
NFR5	PMMA/HEAA5	Yes	NCF

6.3. Result and discussion

6.3.1. Mode-I fracture toughness behavior

The DCB tests were carried out on each configuration, and the typical load-displacement curves are showed in Fig. 25. All configurations performed linear elastic behavior for the initial loading phase, then the curves exhibited nonlinear behavior with a jagged shape until the end of test, linked to unstable crack propagation through the specimen. Even the maximum load value of NFR1 and NFR3 had a negligible difference with V0 configuration, the considerable high values of maximum load were found in the curves of NFR0 and NFR5. Those findings preliminary supposed that the nanofiber modified interlayer had a positive effect on delaying crack initiation, leading to an increase in the maximum load in laminate.

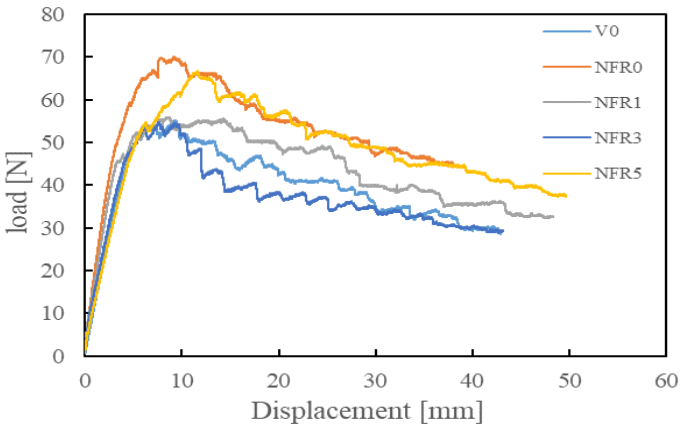

Fig. 25. Typical Mode-I load-displacement curves for CFRTP specimens.

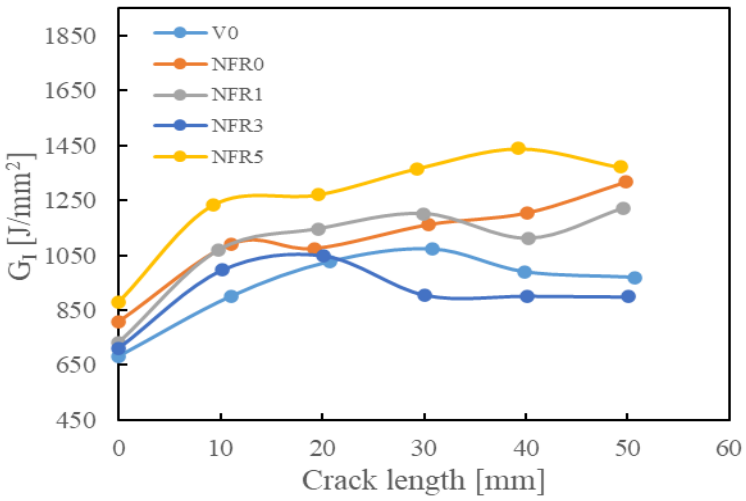

Fig. 26. Typical Mode-I R curves for CFRTP specimens.

According to the MBT method, the G_I has been calculated from the load-displacement data and the incremental crack length. The typical Mode-I R curves plot can be seen in Fig. 26, and the corresponding G_{IC} and G_{IR} were summarized in Table 6. The overall trend for modified configurations was almost the same as for virgin configuration, that is, G_I increased with the crack length growth (Fig. 26). The G_{IC} and G_{IR} of NFR0 configuration were 19.6% and 9% higher than those of the V0 configuration, respectively, as shown in Table 6, indicating that the PA nanofiber interleaving positively affects Mode-I fracture toughness for CFRTPs laminate system. Nevertheless, the modified resin of copolymerization with HEAA exhibited a "decreasing firstly and then increasing" trend on the interlayer toughing effect of PA veils. As the molar concentration of copolymerization with HEAA increased to 3mol%, the G_{IC} and G_{IR} of nanofiber interleaved composite dropped from 19.6%, 9% to 0.7%, -5% compared to V0 respectively. The molar concentration of copolymerization with HEAA increased to 5%, both values of G_{IC} and G_{IR} improved again into 17.6%, 28% in relation to V0, respectively see Table 6. Thus, it was revealed that the fracture

mechanism for the nanofiber interleaved layer was varied with the modification of matrix resin.

Table 6. Experimental results of DCB tests for CFRTP specimens

Specimen	G_{IC}	Δ%	G_{IR}	Δ%
	[J/mm^2]	[%]	[J/mm^2]	[%]
V0	711±26	-	1035±40	-
NFR0	850±48	19.6	1131±39	9
NFR1	733±29	3.1	1151±16	11
NFR3	716±16	0.7	987±53	-5
NFR5	836± 4	17.6	1321±28	28

To further explore the fracture mechanism of DCB specimens, the SEM images of a fracture surface and schematic views of the crack path for each configuration showed in Fig. 27. Some industrial research institutes report that the surface of commercially available CFs is typically designed for interaction with epoxy polymers and not for acrylic polymers such as PMMA [62][63]. Thus, the fracture surfaces of V0 samples appeared to be rough. Brittle fractures of resin and breakages of CF fibers can be observed, indicating that the opening load caused the tensile fracture on the interlayer resin in the thickness direction, and the CFs were also pulled out from the matrix leading to the fiber bridging when the fractured resin debris peeled off the fiber layer(Fig. 27 (a)). For NFR 0 samples, the uneven fracture surface of CFs covered with the local nanofiber rich zone, and pull-out CFs can be noted (Fig. 27 (b)). A nanoscale microphotograph exhibited that the local nanofiber zones contain the plastically deformed PMMA and pull-out nanofibers, as showed in Fig. 29 (a). It was suggested that a crack alternatingly propagates above and below the nanofiber toughened interlayer when a nanofiber veil interleaved. The presence of additional nanofiber bridging led to the higher fracture toughness of the NFR0 samples compared to the V0. However, as the molar concentration of copolymerization with HEAA increased to

3mol%. The nanofiber rich zones almost occupied the fracture surface, which was eventually with few pull-out CFs and fractured matrix (Fig. 27 (c) and (d)), revealed that cracks propagate directly through the nanofiber toughed layer. This phenomenon indicated a conversion of bridging mechanism from the Hybrid bridging of CF and nanofiber to the single bridging of nanofibers, resulting in Mode-I fracture toughness decreased. For the NFR5 specimen, the Hybrid bridging of CF and nanofiber relating to the appearance of an uneven fracture surface with local nanofiber covering reappeared, see in Fig. 27 (e). Moreover, the surface of deboned CFs covered with the resin matrix, indicating the resins deformed before fracture. Consequently, the Mode-I fracture toughness increased again. Based on our finding above, it can be concluded that the change of crack tip path accompanied by the shifting of the bridging mechanism determines the level of Mode-I fracture toughness.

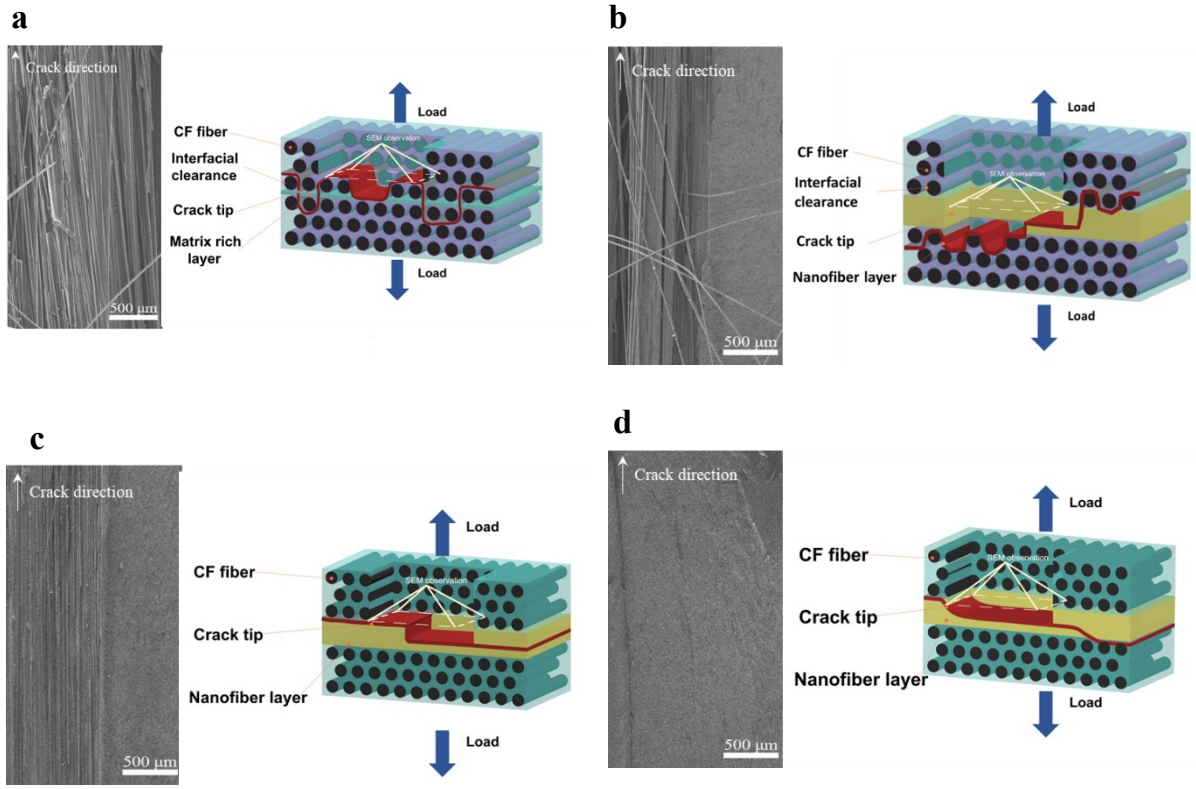

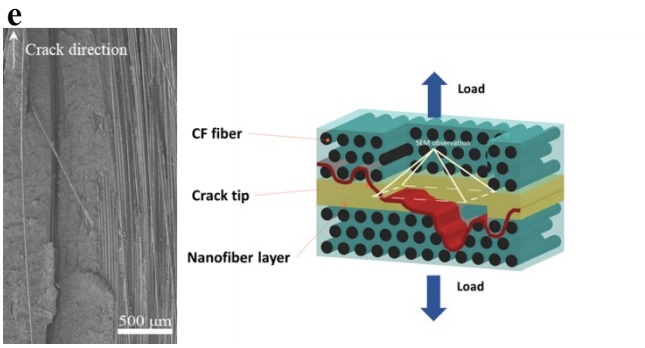

Fig. 27. Typical SEM images of Mode-I fracture surface and schematic views of delamination path for specimen (a) V0, (b) NFR0, (c) NFR1, (d) NFR3, and (e) NFR5.

6.3.2. Interfacial adhesion and toughing mechanism

As the observations mentioned above, the amount changes of HEAA copolymerization have a crucial impact on a change of delamination path under opening load. Thus, the fracture surface of the nanofiber toughened layer and the interface of the CF layer were investigated showed in Fig. 28-Fig. 29 to fully understand the influence of fiber/matrix adhesion and property of modified matrix on the Mode-I toughing mechanism.

For DCB samples, the carbon fiber with smoothness surface was exposed on the fracture surface of the pure PMMA samples (Fig. 28 (a) and (b)). On the contrary, with an increase of the copolymerization concentration with HEAA, the carbon fibers gradually deposited into the matrix (Fig. 28 (c) and (d)). It was suggested that a better adhesion of the resin to the fiber surface in case the resin-modified by copolymerization with HEAA was the reason for the crack propagating above the CF ply. As such, the fewer pull-out CFs was observed (Fig. 27 (c) and (d)), indicating the CFs bridging reduced. Hence, only marginal improvement of G_{IC} and negative effect of G_{IR} compared to the V0 sample. Additionally, Fig. 29 (a) shows that pull-out nanofibers in long and

continuous form remain in the fracture surface of the pure PMMA samples. Since the high displacement of the two interfaces of helves during the DCB experiment results in a higher elongation of the nanofiber. The pull-out of nanofibers ensured that more nanofibers were elongated and break in the sites where far from the crack tip, resulting absorbs more energy. By contrast, fewer pull-out nanofibers on the fracture surface of HEAA copolymerized samples possessed sharp damaged tips, with the main section of nanofibers embedded in the matrix (Fig. 29 (b) and (c)). This phenomenon demonstrated that the improvement of nanofiber/matrix adhesion caused the nanofibers to be broken in a limited elongation range, thereby enabling the small amount of nanofibers bridging to occur only at the tip of the crack, which agrees with [44]. Thus, the fewer CFs bridging, together with a reduction in amount nanofiber bridging upon matrix modification, could negatively affect the Mode-I fracture behavior of laminate. As for the NFR5 sample, although the completely embedding of broken nanofibers in the resin demonstrated less nanofiber bridging (Fig. 29 (d)). Still, a more fractured matrix was attached to deboned CF bundles, indicating that the bonded CF bundles pull out from the CF layer to form a bridging effect due to the low strength and softening of the matrix (Table 4). This explained why G_I of NFR5 rises again compared to V0 samples.

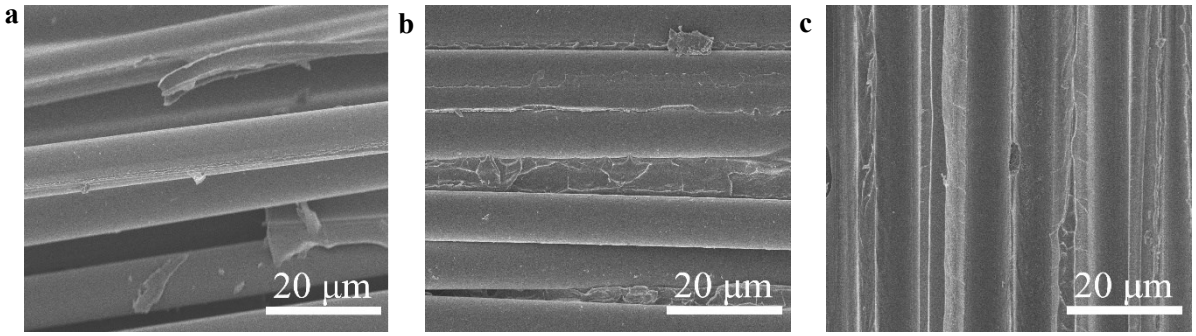

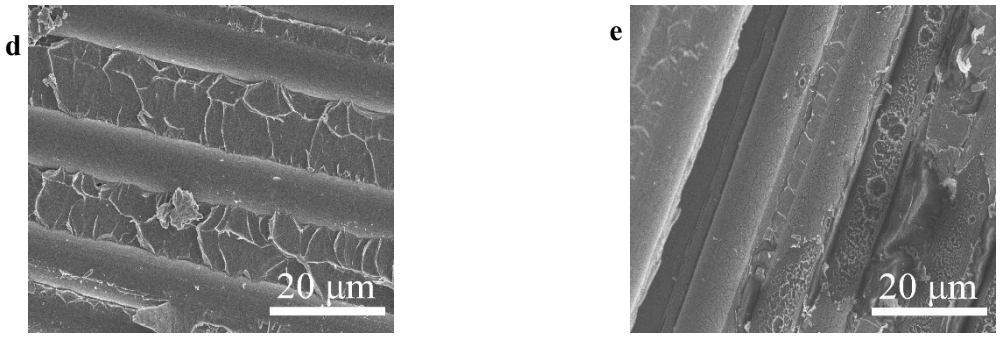

Fig. 28 Typical SEM images of Mode-I fracture interphase of CF layer in specimen (a) V0, (b) NFR0, (c) NFR1, (d) NFR3, and (e) NFR5.

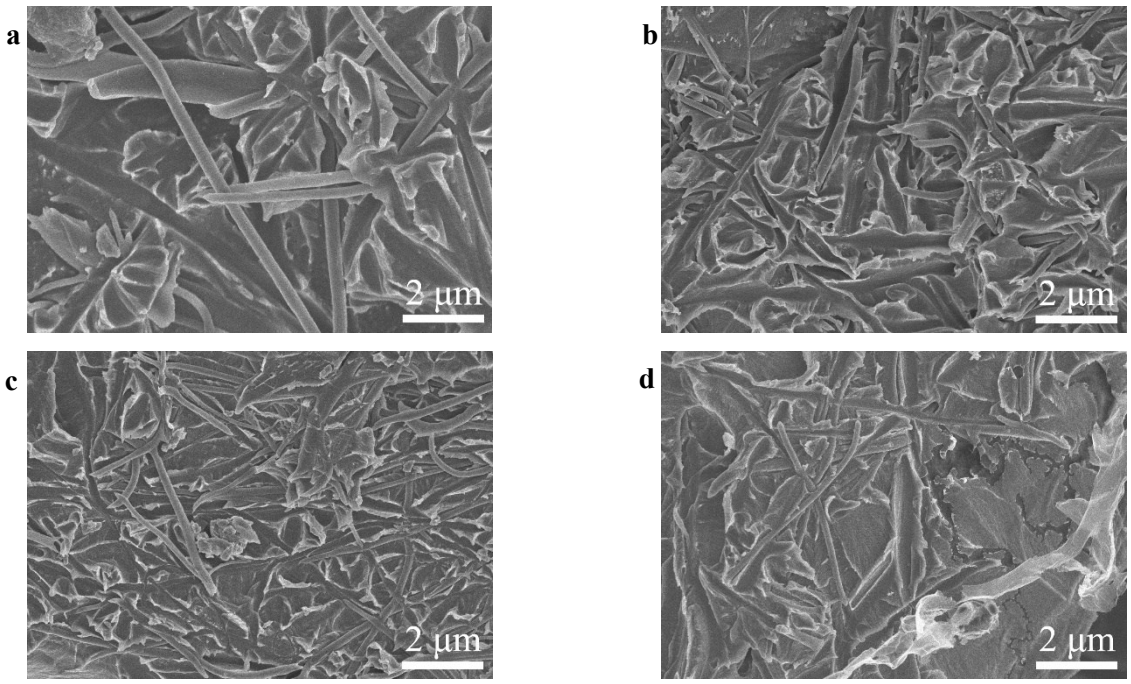

Fig. 29. Typical SEM images of Mode-I fracture surface of nanofiber-toughened layer in specimen (a) V0, (b) NFR0, (c) NFR1, (d) NFR3, and (e) NFR5

6.4. Conclusion

A new attempt has been carried out to apply the electrospun nanofiber to enhance the interlayer toughness of the CFRTP. And based on previous research experience, the different molar concentration of HEAA was copolymerized with MMA, aiming to improve the interfacial adhesion of CF/matrix and nanofiber/matrix in CFRTPs interleaved by PA veils. The data of G_I demonstrated that the interleaved PA veils have

a considerable improvement in interlaminar fracture toughness of the CFRTPs laminate system. But with the increase of HEAA polymerization from 0mol% to 5mol%, the interlayer toughing effect of PA veils exhibited a characteristic of decreasing firstly and then increasing under the Mode-I loading. To further understand the effect of interfacial adhesion on fracture mechanism, we observed the fracture surface of fiber layer and nano-toughing matrix layer in detail. The result showed the improvement of resin adhesion to carbon fiber and PA nanofiber, for the DCB samples, enhanced the interfacial strength between nano-toughing matrix layer and carbon fiber layer, and also greatly inhibited the CF and nanofiber pull out from matrix thereby reducing the bridging effect.

References

[44] Quan D, Deegan B, Alderliesten R, et al. The influence of interlayer/epoxy adhesion on the mode-I and mode-II fracture response of carbon fibre/epoxy composites interleaved with thermoplastic veils. Mater Des. 2020;192:1–10.

[59] Kishi H, Nakao N, Kuwashiro S, et al. Carbon fiber reinforced thermoplastic composites from acrylic polymer matrices: Interfacial adhesion and physical properties. Express Polym Lett. 2017;11:334–342.

[60] JIS K 7086-1993. Testing methods for interlaminar fracture toughness of carbon fiber reinforced plastics. Annu B JIS Stand. 1993.

[61] Japanese Industrial Standards. Testing methods for interlaminar fracture toughness of carbon fiber reinforced plastics. Annu B JIS Stand.

[62] A. Ishitani. Application of X-ray photoelectron spectroscopy to surface analysis

of carbon fiber. Carbon N Y. 1981. p. 269–275.

[63] T. Takahagi AI. XPS studies by use of the digital difference spectrum technique of functional groups on the surface of carbon fiber. Carbon N Y. 1984. p. 43–46.

[64] Liu X, Yang B, Lu L, et al.A thermoplastic multilayered carbon-fabric/polycarbonate laminate prepared by a two-step hot-press technique. Polymers (Basel). 2018;10.

Chapter 7.

Experimental study on Mode-II fracture behavior of nanofiber interleaved CFRTP composites

7.1. Introduction

In the previous chapter, the static flexural tests shows that the interlaminar toughening of nanofibers has good strengthening effect on the flexural behavior of CFRTP laminated system and better inhibits the premature initiation of interlaminar cracks. Thus, the main objective in this chapter was to investigate the mechanisms of Mode-II interlaminar toughness for nanofiber interleaved laminate composites. The PA electrospun nanofiber was chosen as the interleaf material. Furthermore, the compatibility of PMMA resin is typically poor with PA nanofibers and CF fiber. While interfacial adhesion of polymer to CF and nanofiber is the key to realize the potential of interlayer toughing effect of PA nanofiber. Based on the previous research experience[59], the functional monomer hydroxyethyl acrylamide (HEAA) for copolymerization with methyl methacrylate (MMA) was chosen as the modified thermoplastic resin to improve fiber/resin interfacial adhesion. The CFRTP laminate system interleaved with/without nanofiber can be made by the hot-press technique under reasonable hot-press conditions. The Mode-II interlaminar toughness was examined by end notched flexure (ENF) tests. The fracture surface of tested specimens was observed using the scanning electron microscope (SEM). The effects of modified resin copolymerized with different molar concentrations of HEAA on the Mode-II toughness enhancement of nanofiber interleaves was discussed, combined with the test results of the SEM observation.

7.2. Experiments

7.2.1. Prepreg sheet preparation

The materials preparation using this experiment were the same as in chapter 6. These were described in section 6.2.1.

7.2.2. Fabrication of CFRTP laminate

The fabrication of the specimens was the same as chapter 6. The details of molding were explained in section 6.2.2.

7.2.3. Characterization

As recommended in standard JIS K 7086 [61], the ENF tests were performed to investigate the delamination of material in the in-plane shear mode of failure (Mode-II) using a universal test machine fitted with 5kN load cell at a constant displacement rate of 0.5mm/min. The geometry of the ENF specimen was same as DCB tests. The span width was 100mm. In the ENF tests, the levels of critical fracture toughness, which determined by the 5% offset approach according to standard JIS K 7086 (critical energy release rate, G_{IIC}) [61], and propagation fracture toughness which determined at the maximum flexural load have been calculated (propagation energy release rate, G_{IIR}), as given by:

$$G_{II} = \frac{9a_e^2 P^2 C}{2B(2L^3 + 3a_e^3)}$$

where L is the distance between load point and supporter, C is the compliance of ENF specimen, a_e is the effective crack length, that was calculated as:

$$a_e = \left[\frac{C}{C_0}a_0^3 + \frac{2}{3}\left(\frac{C}{C_0} - 1\right)L^3\right]^{\frac{1}{3}}$$

where C_0 is the compliance of the early elastic part. a_0 is the initial crack length.

Since the geometry of ENF specimens was the same as DCB specimens, the details of configuration and specimen type are explained in section 6.2.3

7.3. Result and discussion

7.3.1. Mode-II fracture toughness behavior

In the case of Mode-II loading, the tests were realized by normal flexural experiment, and the typical load-displacement curves can be seen in Fig. 30. A similar smooth non-linear behavior can be identified from the critical point of initial linear behavior to the maximum load of specimen failure, corresponding to crack propagation with a relatively stable stick-slip behavior.

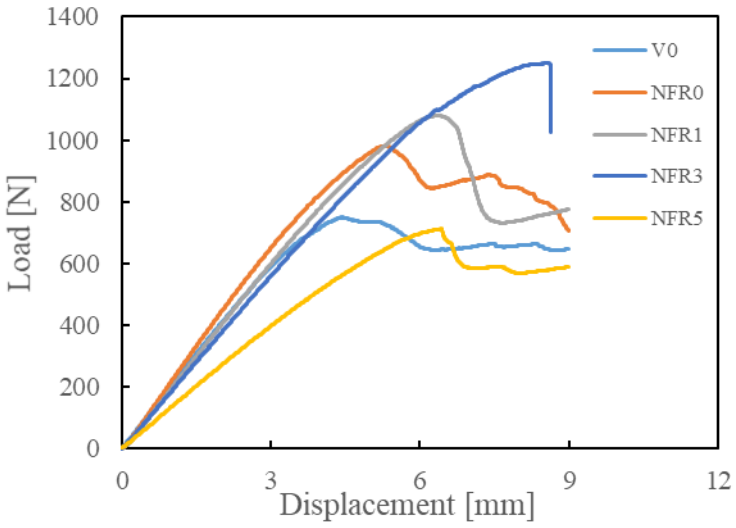

Fig. 30. Typical Mode-II load-displacement curves for CFRTP specimens.

From the ENF tests, the G_{II} has been calculated several times during the tests, the typical Mode-II R curve had been plotted in Fig. 31, and the corresponding fracture energies were summarized in Table 7. All of the configurations exhibited a rising trend, see in Fig. 31. it was found that for the NFR0 configuration, the nanofiber veil interleaving had a negative effect on the G_{IIC} about -29%, on the contrary, which brought with it a massive improvement in G_{IIR} about 85% as a consequence of the nanofiber bridge effect compared to V0 see in Table 7.. Concerning the effectiveness of modified resin copolymerized with the different molar concentration of HEAA on

the interlayer toughing effect of PA veils, the copolymerization with HEAA had a positive and significant relationship with G_{IIC} and G_{IIR} from -29%, 85% for NFR0 to 137%, 147% for NFR3 in relation to V0, respectively; however, the G_{IIC} and G_{IIR} of NFR5 returned to a low value see in Table 7., it was attributed to the elastic modulus of the NFR5 samples dropped sharply with the high molar concentration of copolymerization with HEAA which could be confirmed from the initial elastic region in Fig. 30. It was revealed that modified resin had a positive effect on the interlayer toughing by PA veils under Mode-II loading; However, it was inevitable that the interlaminar toughening effect of PA veils decrease with the degradation weakening of resin properties due to the excessive content of HEAA (Table 4).

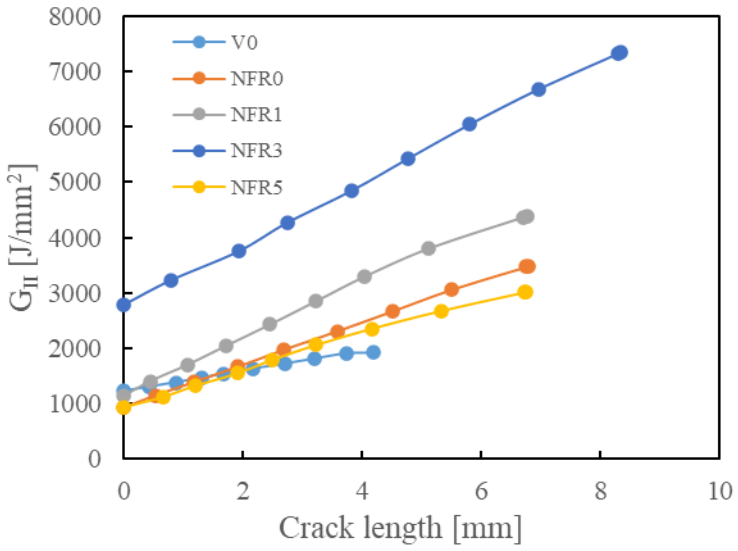

Fig. 31. Typical Mode-II R curves for CFRTP specimens.

The fracture surfaces of ENF samples after Mode-II loading were showed in Fig. 32(a). Smooth and continuous CFs were found from the V0 interface. The crack was mainly located at the interlayer matrix. A combination of hackle formation in the matrix and interfacial failure at CF/matrix suggested the failure mechanism of V0 samples, similar

to previous works [66][67]. With a nanofiber interleaved into the laminate, a distinguishable interlaminar region of the nanofiber toughed layer with a near right-angle edge was presented in the NFR0 laminate (Fig. 32 (b)), which means the crack front passed from one side of interlayer to the other. The nanofiber bridging in the fractured region of the interlayer provided more resistance to the Mode-II crack propagation(G_{IIR}) due to the higher ductility of the PA compared with the resin. But it must be pointed out that the right-angle edge of nanofiber toughed layer and regular CFs surface indicated the microcrack initiation alternated from a cohesive matrix failure to interfacial failure between nanofiber interlayer and CFs. That was the reason why the G_{IIC} decreased. Furthermore, the multilayer shape of deformed nanofiber toughened resin was visible for the fracture surface of NFR1 samples and NFR3 samples (Fig. 32 (c) and (d)), indicating a large amount of nanofiber bridging acted in the thickness direction of the toughened matrix layer. Because under mode II, the two parts of the specimen slide only a few millimeters so that the nanofibers could bear longer load after crack propagation, and the enhancement was much higher than that of the DCB process at each instant [18,68]. Therefore, the Mode-II fracture energy increases greatly. But for the NFR5 samples, the partial crack deviation from toughened interlayer region to interface of CFs and the matrix elastic modulus weakening caused a reduction of fracture energy absorbing (Fig. 32 (e)). Therefore, taking the above observations into account, the appearance of a multilayer microcrack in the nano-toughed layer played a vital role in the improvement of Mode-II toughness.

Table 7. Experimental results of ENF tests for CFRTP specimens

Specimen	G_{IIC} [J/mm^2]	Δ% [%]	G_{IIR} [J/mm^2]	Δ% [%]
V0	1212±23	-	2001±32	-
NFR0	783±79	-29	3396±219	85
NFR1	1131±36	-6	3613±79	89
NFR3	2649±83	137	7815±391	147
NFR5	888±46	-27	3276±251	64

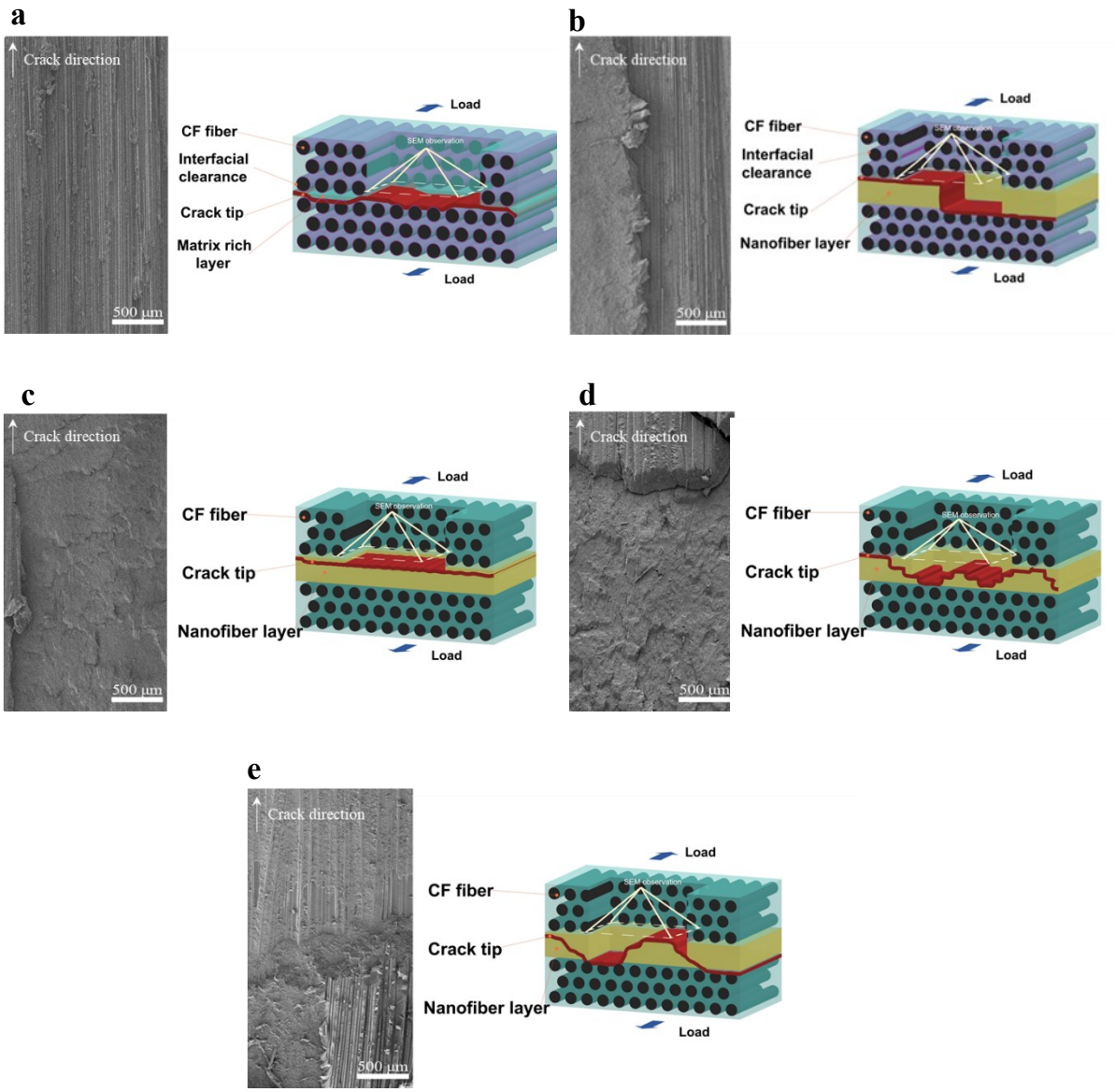

Fig. 32. Typical SEM images of Mode-II fracture surface and schematic views of delamination path for specimen (a) V0, (b) NFR0, (c) NFR1, (d) NFR3, and (e) NFR5.

7.3.2. Interfacial adhesion and toughing mechanism

Section 7.3.1 showed that the amount changes of HEAA copolymerization had a crucial impact on toughening performance for PA nanofiber interleaved laminate systems. In this section, the fracture mechanism of the interleaved laminate was investigated to understand the reasons for causing the significantly varied toughening performance of the PA veils for the different laminate systems.

For the ENF samples, Fig. 33. Typical SEM images of Mode-II fracture interphase of CF layer in specimen (a) V0, (b) NFR0, (c) NFR1, (d) NFR3, and (e) NFR5.(c) and (d) shows that CFs gradually buried with resin, and the plastic deformed resin debris remained on the fiber surface with the molar concentration of HEAA rising compared to pure PMMA samples (Fig. 33(a) and (b)). These phenomena indicated that the path of crack propagation was shifted from interfacial failure between CF and resin to the nanofiber toughed interlayer due to the adhesion enhancement of resin to CFs. Besides, the previous studies showed that the amount of nanofibers involved in the loading process was much higher during ENF test than during a DCB, which was since that in-plane shear forces only result in a limited displacement of crack halves in a specimen [69][70][71], Therefore, the bridging quality of nanofibers, which depends on whether the nanofibers can be effectively strained until fracture as well as the energy absorption in limited displacement, greatly affects the interlaminar toughening effect [72]. This was schematically illustrated in Fig. 35. Where, Nanofibers subjected to a limited amount of straining and do not break due to the nanofiber debone from resin and did not deform in the NFR0 samples and NFR1 samples (Fig. 34 (a)), resulting absorbed a small amount of energy. However, highly irregular and plastically deformed nanofibers protruding from the resin could be identified in NFR3 samples (Fig. 34 (c)), indicating

that it was difficult for the nanofibers to debond from the matrix, leading to a sufficient fracture strain on the nanofibers and would be able to absorb more energy. Finally, it must be noted that the insufficient polymeric HEAA component led to an excessive plasticization of the matrix for NFR5 samples, resulting in resin destruction with a state of high deformation, low tensile strength, and inhibition of nanofiber rupture work. Here, as is well known, bulk polymerization is easy to generate unreacted monomer components, such as the HEAA component above. Therefore, This could be proved by the macroscale deformation of covering resin on the fiber surface (Fig. 33 (e)) and the deep embedding of broken nanofibers into the matrix resin (Fig. 34 (d)).

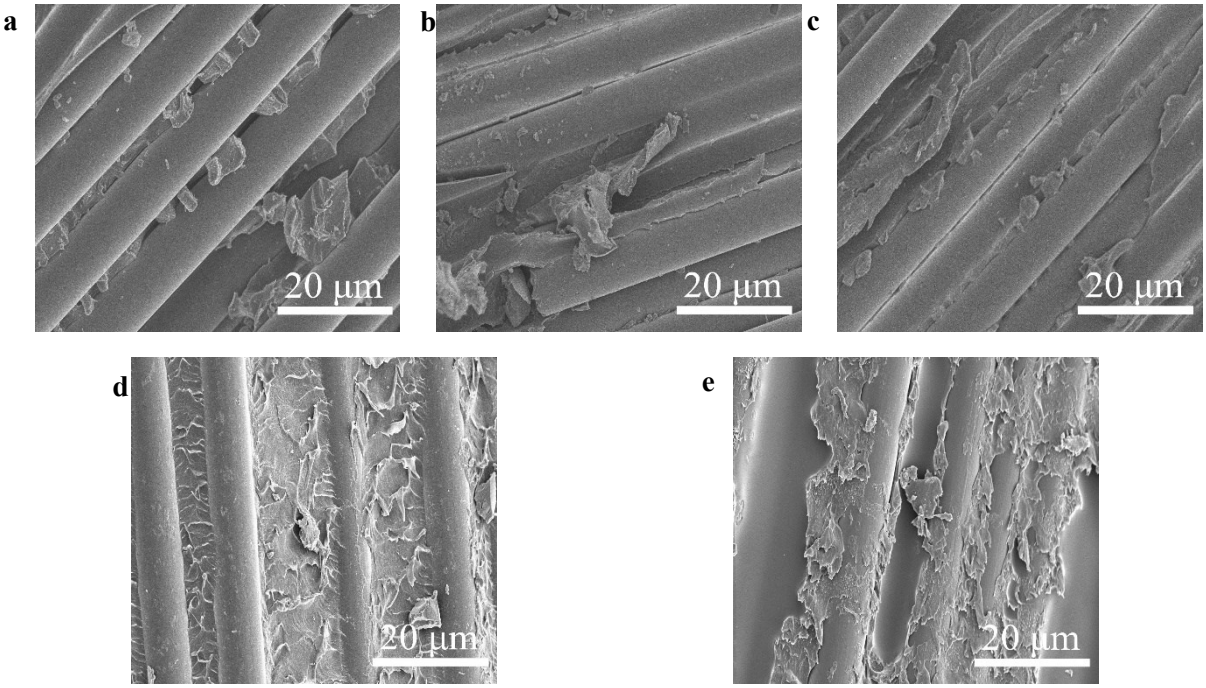

Fig. 33. Typical SEM images of Mode-II fracture interphase of CF layer in specimen (a) V0, (b) NFR0, (c) NFR1, (d) NFR3, and (e) NFR5.

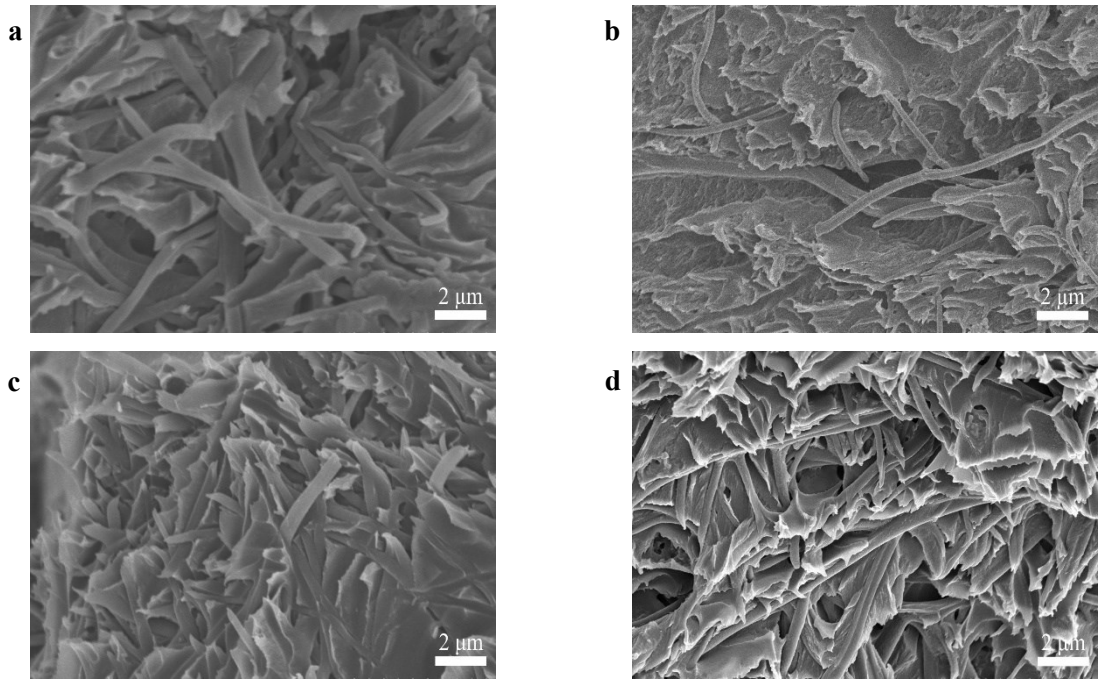

Fig. 34. Typical SEM image of Mode-II fracture surface of nanofiber-toughened layer in specimen (a) V0, (b) NFR0, (c) NFR1, (d) NFR3, and (e) NFR5.

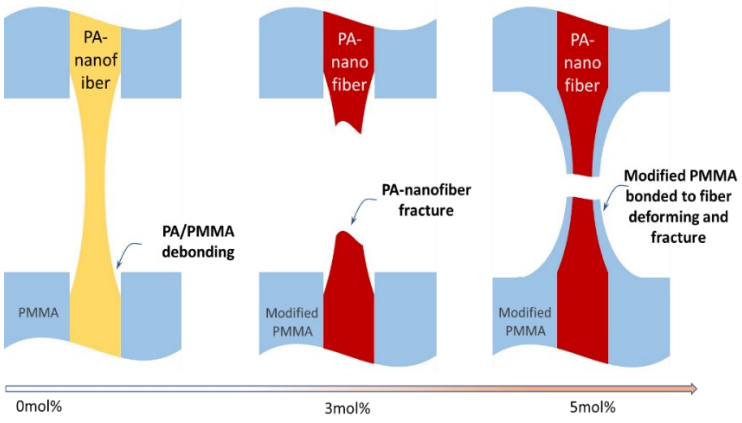

Fig. 35. Simplified representation of the rupture work of the PA-fiber composite under tensile loading

7.4. Conclusion

In this work, the Mode-II fracture behavior of CFRTP interleaved with PA veils was studied; the data G_{II} demonstrated that the interleaved PA veils had a considerable improvement in interlaminar fracture toughness of the CFRTPs laminate system. But with the increase of HEAA polymerization from 0mol% to 5mol%, the interlayer toughing effect of PA veils exhibited a characteristic of increasing firstly and then

decreasing, which was related to the formation of multilayer microcrack in nano-toughing matrix layer.

To further understand the effect of interfacial adhesion on fracture mechanism, we observed the fracture surface of the fiber layer and nano-toughing matrix layer in detail. For the ENF samples, the result showed the improvement of resin adhesion to carbon fiber, and PA nanofiber effectively enhanced shear stress transmission between nanofiber and matrix and made the nanofibers have more effective fracture work without debonding, thereby improving the bridging quality of nanofibers. But it must be pointed out that the insufficient polymeric HEAA component also made the resin too elastic when the high content of HEAA feed in bulk polymerization, resulting in insufficient deformation strength.

References

[18] Daelemans L, Van Der Heijden S, De Baere I, et al. Damage-Resistant Composites Using Electrospun Nanofibers: A Multiscale Analysis of the Toughening Mechanisms. ACS Appl Mater Interfaces. 2016;8:11806–11818.

[59] Kishi H, Nakao N, Kuwashiro S, et al. Carbon fiber reinforced thermoplastic composites from acrylic polymer matrices: Interfacial adhesion and physical properties. Express Polym Lett. 2017;11:334–342.

[61] Japanese Industrial Standards. Testing methods for interlaminar fracture toughness of carbon fiber reinforced plastics. Annu B JIS Stand.

[66] Todo M, Jar PYB, Takahashi K. Initiation of a mode-II interlaminar crack from an insert film in the end-notched flexure composite specimen. Compos Sci Technol. 2000;60:263–272.

[67] Robinette EJ. Toughening Vinyl Ester Matrix Composites by Tailoring Nanoscale and Mesoscale Interfaces. PhD Diss 2006. 2005;

[68] Saghafi H, Palazzetti R, Zucchelli A, et al. Influence of electrospun nanofibers on the interlaminar properties of unidirectional epoxy resin/glass fiber composite laminates. J Reinf Plast Compos. 2015;34:907–914.

[69] Palazzetti R, Yan X, Zucchelli A. Influence of geometrical features of electrospun nylon 6,6 interleave on the CFRP laminates mechanical properties. Polym Compos. 2014;35:137–150.

[70] Moroni F, Palazzetti R, Zucchelli A, et al. A numerical investigation on the interlaminar strength of nanomodified composite interfaces. Compos Part B Eng [Internet]. 2013;55:635–641. Available from: http://dx.doi.org/10.1016/j.compositesb.2013.07.004.

[71] Giuliese G, Palazzetti R, Moroni F, et al. Cohesive zone modelling of delamination response of a composite laminate with interleaved nylon 6,6 nanofibres. Compos Part B Eng [Internet]. 2015;78:384–392. Available from: http://dx.doi.org/10.1016/j.compositesb.2015.03.087.

[72] van der Heijden S, Daelemans L, De Bruycker K, et al. Novel composite materials with tunable delamination resistance using functionalizable electrospun SBS fibers. Compos Struct [Internet]. 2017;159:12–20. Available from: http://dx.doi.org/10.1016/j.compstruct.2016.09.057.

Chapter 8.
Summary of conclusions and future work

8.1. Summary of research work

The application and mechanism characterization of nanofibers for interlaminar toughening of composite materials was studied by two main aspects, including the influence of interlaminar toughing using nanofiber veils on static/fatigue properties and mechanisms of CFRP; applied the nanofiber veil to toughing the fracture toughness of CFRTP. The research works were summarized as follows: In chapter 1, the background of the wide application of laminated composite systems and the problems in the failure of laminated composite systems are given. The importance of our work was highlighted by reviewing previous work on toughening, interlaminar toughness testing, and post-impact compression properties of composites. The flexural static and fatigue behavior of nanofiber veil toughed cross-ply CFRP laminates were described and evaluated in chapters 2, 3, 4. In chapters 5, 6, 7, the mechanisms of static flexural behavior, Mode-I and Mode-II interlaminar toughening by nanofiber veils for CFRTP were characterized and assessed,in addition the effects of interfacial adhesion improvement of fiber/matrix on the effect of nanofiber interlayer toughness enhancement was discussed in detail. In chapter 8, the final conclusions of this thesis and future work are mentioned and suggested.

8.2. Conclusion on fabrication of specimens

This work confirmed that PA nanofiber veils as interleaf materials were valid for the VaRTM method. Molding of voidless panels could be realized. The Vf of specimens was about 50 vol%. Besides, the PA nanofiber interleaved CFRTP laminate system was firstly fabricated by hot-press technology. The hot-press condition was decided by the

DSC analysis of PA nanofiber, which confirmed that the melting point of PA nanofiber was 186 ℃, the fiber volume fraction of prepreg sheet is about 48%, And the Vf of nano-modified and virgin CFRTP sample was about 50.3%, 51.5%,respectively. This phenomenon indicated that The influence of single layer nanofiber veil as the nanoreinforce inserted into the interlayer on the Vf of the final manufactured can be negligible due to their ultra thin-film characteristics

8.3. Conclusion on test program

Fiber reinforced composites in polymer matrix offer substantial improvements over metals not only for the high specific stiffness and strength, but also for their resistance to fatigue. In particular, as well documented in the open literature, the fiber reinforced composite progressive degradation of material property that accompanies fatigue cycling, was a very interesting feature when compared with the sharp degradation right before failure experienced with steel. Thus quantitative information about damage accumulation and property degradation of nanofiber interleaved CFRP laminate during cycling is necessary for analysis, design, and life prediction to ensure reliability in service applications. Furthermore, design requirements may be focused on acceptable levels of stiffness loss over the component lifetime rather than on material failure. In our study, the RFS parameter provides a quite convenient method to the monitoring of material stiffness; data presented in the RFS parameter versus the number of cycles allow us to determine the level of fatigue loading with respect to static strength, knowing the acceptable level of stiffness degradation within a given number of cycles. Alternatively, if a fatigue loading level is specified, it is possible to determine a given critical stiffness loss by the number of cycles.

Because one feature of laminate materials is their layered construction of stacked plies, delamination is a common failure mode. From both material science and engineering design standpoints, the understanding of the physical origin of composite delamination and the theoretical modeling for delamination fracture toughness are necessary. Therefore, the DCB and ENF tests were selected as the Mode-I and Mode-II interlaminar toughness tests. Both tests were carried out based on JIS standards. The parameter of energy release rate G was divided into two periods, including G_C and G_R, in both test programs, which were convenient to analyze the energy required of crack initiation and crack propagation.

8.4. Conclusion on improvement by electrospun nanofiber as interleaf materials

A nanofiber interleaved CFRP composite material laminate has been characterized for its fatigue behavior. The selected composite is characterized by a particular type of nanomodification as in each interface between 0°- and 90°- oriented plies interleaved the PA nanofiber.

The reduction in stiffness and strength for cross-ply was investigated over a wide range of bending fatigue loading. The experimental results point out the following conclusions: in ILSS and static flexural tests, for the virgin specimen, failure was associated with tensile failure of an inner core of 90° layer. In nanomodified specimen, shear failure of the nanofiber interleaved layer was observed, these mechanisms change to lead the ILSS and UFS of nano-modified configuration was higher than virgin ones; when considering the stiffness loss during cycling, nanomodified specimens were observed to suffer less losses than virgin specimens at fatigue loading up to 40%~75% UFS. At higher fatigue loading, virgin specimens damage more than nanomodified

specimens. This was attributed to the different damage mechanisms for the two specimens; when looking at the rate of stiffness loss during fatigue cycling, data were quite similar for the two sets of specimens up to 50% UFS. For higher levels for the fatigue loading, the range of stiffness loss was less pronounced for nanomodified specimens; the traditional S-N plotting indicated that the fatigue stress range for nanomodified specimens was more spread for virgin ones. Moreover, the maximum valuer of fatigue strength of nano-modified configuration was 1.7 times higher than virgin configuration.

The fracture behavior of CFRTP interleaved with PA veils was studied, with the fiber/matrix adhesion significantly improved upon applying modified thermoplastic resin, which obtained by using functional monomer hydroxyethyl acrylamide (HEAA) for copolymerization with methyl methacrylate (MMA). Two laminate systems were manufactured by hot-press of unidirectional (UD) prepregs, as they exhibited significantly different fracture energies and mechanisms. The different fracture behavior and mechanisms of the non-modified laminates resulted in a significantly different toughening performance of the nanofiber interleaved samples. For the Mode-I loading, applying the different molar concentrations of functional monomer to the nanofiber interleaved configuration resulted in the change of delamination path accompanied by the shifting of bridging mechanism, and subsequently led to a characteristic of decreasing first and then increasing in Mode-I fracture energies. For the Mode-II loading exhibited a characteristic of increasing first and then decreasing, which was related to the formation of multilayer microcrack in the nano-toughing matrix layer. Additionally, the enhanced fiber/matrix adhesion upon the resin

modification inhibited the fiber bridging under opening loading, which caused deteriorations in the Mode-I fracture behavior of the laminate and enhanced the interfacial shear stress transmission under in-plane shear loading, which caused improvement in Mode-II fracture behavior of the laminate, during the fracture process. This work revealed obvious effects of the fiber/matrix adhesion on the fracture behavior of interleaved laminates, and moreover, these effects significantly varied in different CFRTP systems.

8.5. Future work: Effect of cold plasma surface treatment on toughening mechanisms responsible for crack resistance in thermo-plastic nanofiber reinforced epoxies.

In fact, electrospinning has been increasingly used in the manufacture of nonwoven nanofibers. Indeed, it is one of the most versatile and cost-effective technologies with good results and repeatability[73]. In particular, the addition of thermoplastic electrospun nanofibers to toughen epoxy composite has attracted research interest because they have certain advantages, such as nanoporous structure, high surface to volume ratio, and can be made from a variety of polymer materials[74]. However, many factors also affect the toughing performance of the nanofiber veils, mainly focusing on the surface density of veils[20], the materials of the veils[18,19], the form of the veils, i.e., melted or unmelted[18]. Although the influence of these factors has been proved to be crucial. It should be pointed out that electrospun fibers had low compatibility with epoxy resin clearly, the adhesion level between the thermoplastic nanofiber veils and epoxy matrix was another important factor that often seriously affects the toughening performance of nanofiber veils[48].

To limit the drawback mentioned above, previous research (chapter 5, 6, 7) has studied and discussed the modified resin copolymerized with different molar concentrations of functional monomer on the toughening effect of PA nanofiber veils. It is undeniable that the modified resin has a good effect on the enhancement of fiber/resin interface adhesion, whereas, the polymerization of functional monomers also leads to irreversible changes in the mechanical properties of the modified resin. Thus, surface treatment regard with cold plasma is a good potential candidate for the surface modification of polymer nanofibers. Because of the low pressure and power of the cold plasma source, it had a relatively low processing temperature, which allows cold plasma to deal with temperature-sensitive materials (Fig. 36); in addition, cold plasma treatment is non-contact, which can avoid secondary damage to the treated material[75,76].

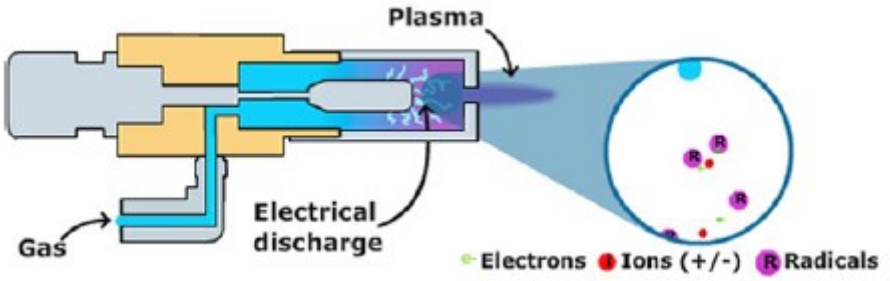

Fig. 36. Schematic representation of cold plasma treatment.

Thus, the future work mainly enables the use of cold plasma technology with various active gas (NH3, O2, N2) to activate the surface of thermoplastic veils and examine surface chemistry variations by using X-ray photoelectron spectroscopy (XPS), thereby significantly improving the adhering of nanofiber/epoxy resins. Subsequently, single edge notched specimens are manufactured through the procedure, as shown in Fig. 37. The influence of the adhesion/epoxy resins on the fracture behavior of nanofiber reinforced epoxy resin was investigated by tension experiments on single notched

specimens. The fracture behavior based on load-extension data from single edge notched tension experiments are analyzed, and calculate the opening fracture toughness by an approach of numerically defined a relevant fracture. The mechanisms change in the plasma-treated material is clarified by microscopic analysis combined with the fracture toughness data. Finally, The Discussion about the correlation between the parameter of cold plasma and the fracture toughness of nanofiber toughened epoxy composite will be launched.

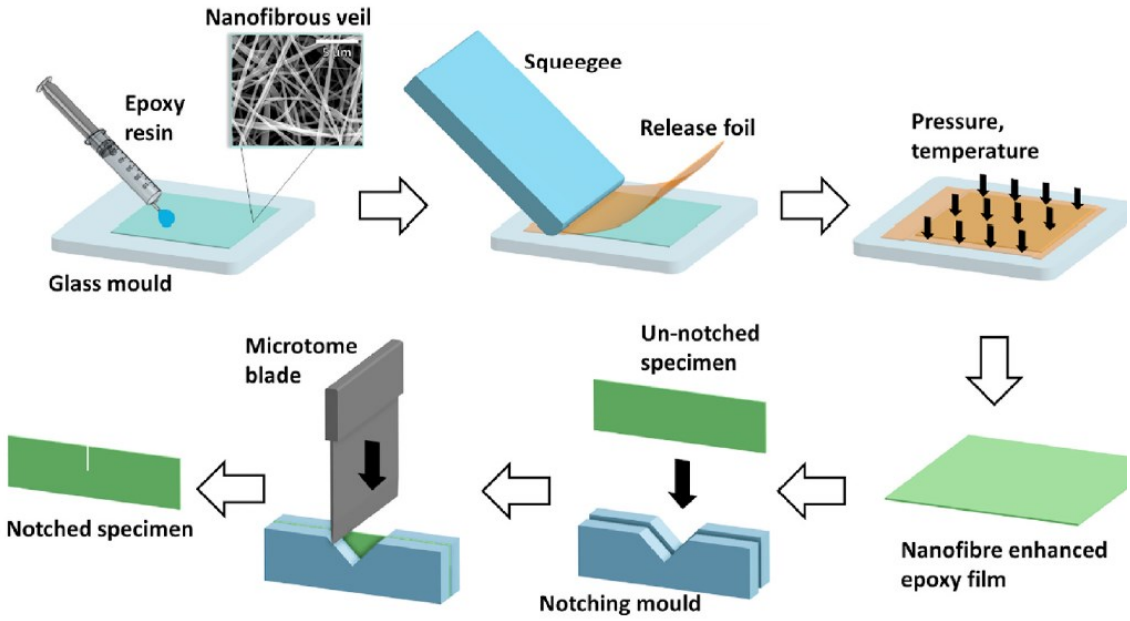

Fig. 37. Schematic view of the production route used to obtain thin nanofiber modified epoxy SENT specimens.

References

[18] Daelemans L, Van Der Heijden S, De Baere I, et al. 16Damage-Resistant Composites Using Electrospun Nanofibers: A Multiscale Analysis of the Toughening Mechanisms. ACS Appl Mater Interfaces. 2016;8:11806–11818.

[19] Ramirez VA, Hogg PJ, Sampson WW. The influence of the nonwoven veil architectures on interlaminar fracture toughness of interleaved composites. Compos Sci Technol [Internet]. 2015;110:103–110.

[20] Beckermann GW, Pickering KL. Mode i and Mode II interlaminar fracture toughness of composite laminates interleaved with electrospun nanofibre veils. Compos Part A Appl Sci Manuf. 2015;72:11–21.

[48] Kinloch AJ, Kodokian GKA, Watts JF. Relationships between the surface free energies and surface chemical compositions of thermoplastic fibre composites and adhesive joint strengths. J Mater Sci Lett. 1991;10:815–818.

[73] Shi X, Zhou W, Ma D, et al. Review Article Electrospinning of Nanofibers and Their Applications for Electrospinning of Nanofibers and Their Applications for. 2015;2015.

[74] Huang ZM, Zhang YZ, Kotaki M, et al. A review on polymer nanofibers by electrospinning and their applications in nanocomposites. Compos Sci Technol. 2003;63:2223–2253.

[75] Dufay M, Jimenez M, Degoutin S. Effect of Cold Plasma Treatment on Electrospun Nanofibers Properties: A Review. ACS Appl Bio Mater. 2020;3:4696–4716.

[76] Zaldivar RJ, Steckel GL, Morgan BA, et al. Bonding optimization on composite surfaces using atmospheric plasma treatment. J Adhes Sci Technol

Acknowledgments

This work was carried out at Gifu university, graduate school of Engineering.

A number of people offered their support to make the project a success. I would like to express my thanks to my supervisors, Professor Asami Nakai, Professor Akiyoshi Takeno, and Assist Professor Shiya Takahashi for their useful comments, suggestions, and encouragement.

Many thanks also to Mrs. Eri Minowa, Mr. Aki Fudawuti, for their support for the experiment, advice, and help.

Thanks also to my composite group colleagues for their support and light conversations.

Finally, I would like to thank my mother and girlfriend for their selfless help and support in study and life, which makes me full of hope and gratitude for the future. Also, thanks my dear father in heaven for blessing me more courageously to face difficulties and challenges.